AMERICAN UNIVERSITY OF BEIRUT

NON-SINGULAR BLACK HOLE IN ASYMPTOTICALLY FREE MIMETIC GRAVITY

by
MARIAM IMAD KHALDIEH

A thesis
submitted in partial fulfillment of the requirements
for the degree of Master of Science
to the Department of Physics
of the Faculty of Arts and Sciences
at the American University of Beirut

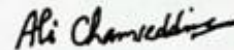Beirut, Lebanon
January 2021

AMERICAN UNIVERSITY OF BEIRUT

NON-SINGULAR BLACK HOLE IN ASYMPTOTICALLY FREE MIMETIC GRAVITY
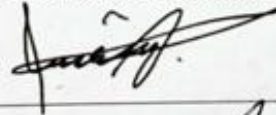
by
MARIAM IMAD KHALDIEH

Approved by:

Dr. Ali Chamseddine, Professor

Department of Physics

Advisor
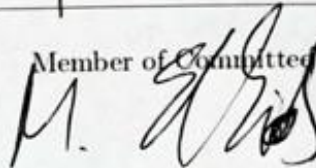
Ali Chamseddine

Dr. Jihad Touma, Professor

Department of Physics

Member of Committee

Dr. Mounib El Eid, Professor

Department of Physics

Member of Committee

Date of thesis defense: January 27, 2021

AMERICAN UNIVERSITY OF BEIRUT

THESIS, DISSERTATION, PROJECT
RELEASE FORM

Student Name: __Khaldieh__ __Mariam__ __Imad__
            Last   First   Middle

☑ Master's Thesis   ◯ Master's Project   ◯ Doctoral Dissertation

☐   I authorize the American University of Beirut to: (a) reproduce hard or electronic copies of my thesis, dissertation, or project; (b) include such copies in the archives and digital repositories of the University; and (c) make freely available such copies to third parties for research or educational purposes.

☑   I authorize the American University of Beirut, to: (a) reproduce hard or electronic copies of it; (b) include such copies in the archives and digital repositories of the University; and (c) make freely available such copies to third parties for research or educational purposes after: **One** ___ **year from the date of submission of my thesis, dissertation or project.**
      Two ___ **years from the date of submission of my thesis , dissertation or project.**
      (Three) ___ **years from the date of submission of my thesis , dissertation or project.**

___M. Xargue___   February 7, 2021
     Signature   Date

This form is signed when submitting the thesis, dissertation, or project to the University Libraries

Acknowledgements

I would first like to thank my dear advisor Professor Ali Chamseddine for his guidance and unique pedagogical approach. I still remember when I was an undergraduate, he always encouraged me to challenge myself with advanced courses, and continued to do so later throughout my graduate studies and thesis work as well, and thanks to him I am now an independent budding researcher. Our discussions helped me build a vision in modified gravity and learn about problems that are at the heart of the field. I am grateful to him for putting up with my complaints on papers, equations, and a multitude of things I never liked, and that throughout my fluctuations he was a solid ground and reference. I look up to his ingenuity and hope to become a successor that he is proud of.

I especially thank Prof Jihad Touma, who adopted me into the Physics department when I was running away from my Biology undergrad major. His guidance was invaluable for me to learn, adjust and grow not only as a physicist but as a person. No words can describe my gratitude to him as a mentor and a friend. Our countless discussions and shared appreciation for the geometrical approach in problems are the ground on which I stand on today. I learned to like it so much that I went to Professor Ali to work on the lines of his geometrical Dark Matter theory.

I also want to thank Prof Leonid Klushin who was a positive force in my studies and for always keeping me in check on physical intuition and thorough understanding of concepts. I am lucky I got to sit in his classes and learn from him, he is a school in pedagogy and at all.

I thank my dearest friends Sarah, Hana and Rod for endless support, and Rod for giving me a few day-crash course in MATLAB.

I thank Mohammad for being my companion through it all.

I thank mom and dad who supported me throughout without knowing, till this day, what am I working on.

Finally I want to thank God and myself for finishing this thesis. My fear that Prof Ali will get tired of me was the main drive for completing this work.

An Abstract of the Thesis of

Mariam Imad Khaldieh for Master of Science
  Major: Physics

Title: Non-Singular Black Hole in Asymptotically Free Mimetic Gravity

In General Relativity the works of Hawking and Penrose have shown that singular solutions are in-avoidable. The most famous of which are the Schwarzschild and Kerr black hole solutions and Friedman Cosmological solution. In 2013, Chamseddine and Mukhanov have proposed a theory of gravity, with minimal modification where the scale factor is exchanged with a constrained scalar mode that plays the role of time coordinate. The modification is minimal in the sense that the new theory has only additional half degree of freedom corresponding to the presence of dark matter in the form of dust, and thus the name "mimetic gravity". And in recent work, Chamseddine, Mukhanov and Russ, have obtained exact non-singular black hole (NSBH) and cosmological solutions, and this thesis addresses the Schwarzschild-like NSBH solution.

In this work, we study in detail the properties of the Schwarzschild-like solution near time t=0 showing how the singularity is avoided. In addition, and more importantly we study motion near the horizon, where particles curiously oscillate in and out of the horizon. The study also explores the whole spectrum of dynamics for massive and massless particles alike, and new results arise in contrast to the regular Schwarzschild solution. We find a new class of bound orbits for such particles with non-zero angular momentum, orbiting across the internal and external regions of the non-singular black hole, all the while avoiding any physical contradictions. A particularly interesting result obtained was stable photon orbits in the inner region of space-time metric. And even though it was found that black hole evaporation yields a stable black hole remnant of minimal mass, this work studies dynamics in the limit where the mass is less than that of a minimal black hole remnant. And while this limit is not prohibited in the theory, it has a prominent feature: the absence of horizons, implying that any additional dynamical features are potentially observed.

Contents

List of Figures

Chapter 1

Introduction

It is not an exaggeration to say that the major scientific triumph during this past year was establishing that black holes can form within the theory of general relativity, through the discovery of a supermassive compact object at the center of our galaxy, compatible with a black hole, which was awarded the Nobel Prize in Physics [3]. What is involved is not just the discovery of yet another extremely remarkable astrophysical object, but a test of the correctness of our understanding of the properties of space and time in extremely strong gravitational fields. It is even more remarkable to think that such a discovery could hold in itself, not only a major test to the theory of general relativity as we know it, but also the limit to which it is applicable, and provide the window through which we explore what lays *beyond the general theory of relativity.*

The idea that a dark object, with an escape velocity larger than the speed of light, exists, dates back to 1700s, when English astronomerJohn Michell (1783) calculated that a star with the same density as the Sun, but a radius 500 times as large, would have a gravitational pull so strong that light would not be able to escape. In 1796, Laplace independently made a similar suggestion in his *Exposition du Système du Monde.* These objects that were contemplated by Michell and Laplace would now be classified as supermassive black holes, with a mass comparable to that of the compact object at the center of our galaxy.

Over-a-hundred years later, 13 January 1916 would go down in history as the day the first solution to Einstein's equation was found, by the German astronomer Karl Schwarzschild. His solution describes the curved space-time around a spherically symmetric non-rotating mass, with a metric of the form

$$ds^2 = \left(1 - \frac{2GM}{c^2 r}\right)c^2 dt^2 - \left(1 - \frac{2GM}{c^2 r}\right)^{-1} dr^2 - r^2(d\theta^2 + sin^2\theta \ d\phi^2)$$

For years to come, the intriguing features of the metric at positions $r = 0$ and $r = \frac{2GM}{c^2}$ were a subject of confusion in terms of interpreting the metric. It was

only later when researches determined that $r = 0$ is a true 'singularity', while $r = \frac{2GM}{c^2}$ point was only an artifact caused by the choice of coordinates.

Later in 1965, Penrose proceeded to prove that collapsing matter with positive energy density forms a *trapped surface*, beyond which it is impossible to prevent further collapse, leading to an inevitable 'singularity'. This result, regarded as the first important post-Einsteinian result in general relativity, triggered a new era in physics and astronomy. Later, Penrose together with Stephen Hawking, went further to show that similar results applied to cosmological singularities [4]. Their proof that space-times describing such as, for instance, Friedmann and Kasner universes and black holes, are geodesically incomplete carried a rather physically unappealing interpreration. The requirement of causal geodesic completeness is simply that every timelike and null geodesic can be extended to arbitrarily large affine parameter value, both into the future and into the past. In crude terms we could interpret this condition as saying: 'photons and freely moving particles cannot just appear or disappear off the edge of the universe' [4]. A completeness condition of this kind is sometimes used as virtually a *definition* of what is meant by a non-singular space-time [cf. Geroch 1968a]. This opens the discussion on *'resolving singularities'*, where regular solutions for Einsteins equations are sought-that are geodesically complete.

Later on, profound links were found between black hole theory and such seemingly very distant fields as thermodynamics, information theory, and quantum theory. It became well known that when the curvature approaches the Planckian value quantum effects become extremely important and Einstein theory must be modified, and such a modification to the theory of gravity as we know it, was sought in a unification between quantum and gravity theory on Planckian scales. However, the progress along this line of research has been relatively modest in spite of the enormous efforts devoted to the problem, and therefore the "quantum resolution" of singularities remains rather obscure.

There are, of course, different "non-quantum" approach to resolving the singularities. Creative efforts in that direction yielded interesting speculations. One can imagine that, at high curvatures, classical General Relativity is modified to incorporate the idea of *limiting curvature* as to avoid divergence at $r = 0$ [5]. Another attempt to resolve singularities was by implementing the idea of an *asymptotic disappearance of gravitational interactions of matter* [6]. An attempt, which incorporates both ideas, was discussed in recent work of Chamseddine, Mukhanov and Russ [2], whose resulting non-singular solution is the main focus of this work. While their work will occupy a fair part of the literature, the thesis is structured in the following way: The second chapter studies, in depth, the problem of singularity specific to the Schwarzschild black hole, which will set the ground for the analysis to be done later on the non-singular Schwarzschild-like solution obtained

in [2]. The third chapter will discuss the derivation of the non-singular solution obtained in the framework of Chamseddine and Mukhanov's mimetic gravity theory, reaching the metric solution of the non-singular black hole. The fourth chapter will study, in detail, the solution obtained, and a discussion along the one carried in the Schwarzschild case will be presented (Sec.4.1), first showing how the singularity is avoided in such a space-time (Sec.4.4), then highlighting interesting features of motion near the horizon (Sec.4.5), and giving a semi-qualitative treatment of particle motion in the non-singular geometry (Sec.4.6), taking the different mass limits presented in the theory (Sec.4.7 and 4.8).

Chapter 2

The Singularity Problem

While 'singularities' can be broadly divided into three classes: past-spacelike (like in white holes or the big bang), timelike (naked singularities), and future-spacelike singularities (black holes), we will focus in the first sections on the Schwarzschild black hole, to lay out its features in details, then move into a more general framework on singularity theorems and ways to resolve them.

2.1 The Schwarzschild Metric

That the Schwarzschild geometry is relevant to gravitational collapse follows from *Birkhoff's (1923) theorem* which states [1]:

Let the geometry of a given region of space-time (1) be spherically symmetric, and (2) be a solution to the Einstein field equations in vacuum. Then that geometry is necessarily a piece of Schwarzschild geometry.

The external field of any electrically neutral, spherical star satisfies the conditions of Birkhoff's theorem, whether the star is static, vibrating, or collapsing. Therefore the external field must be a piece of the Schwarzschild geometry.

Birkhoff's theorem is also easy to prove. Condsidering a spherical region of space-time, where on can introduce Schwarzschild coordinates:

$$ds^2 = -e^{2\Phi}dt^2 + e^{2\Lambda}dr^2 + r^2(d\theta^2 + sin^2\theta \ d\phi^2) \qquad (2.1)$$

where

$$\Phi = \Phi(t, r), \quad and \quad \Lambda = \Lambda(t, r)$$

By imposing Einstein's vacuum field equations on the metric (2.1), components of the Einstein tensor can be given by

$$G_{tt} = r^{-2}(1 - e^{-2\Lambda}) + 2(\Lambda_{,r}/r)e^{-2\Lambda} = 0, \tag{2.2}$$

$$G_{tr} = G_{rt} = 2(\Lambda_{,t}/r)e^{-\Lambda+\Phi} = 0, \tag{2.3}$$

$$G_{rr} = r^{-2}(e^{-2\Lambda} - 1) + 2(\Phi_{,r}/r)e^{-2\Lambda} = 0, \tag{2.4}$$

$$G_{\theta\theta} = G_{\phi\phi} = (\Phi_{,rr} + \Phi_{,r}^2 - \Phi_{,r}\Lambda_{,r} + \Phi_{,r}/r - \Lambda_{,r}/r)e^{-2\Lambda} - (\Lambda_{,tt} + \Lambda_{,t}^2 - \Lambda_{,t}\Phi_{,t})e^{-2\Phi} = 0 \tag{2.5}$$

Solutions to Λ and Φ following from the above equations are hence given by

$$\Lambda = -\frac{1}{2}ln|1 - 2M/r| \tag{2.6}$$

and

$$\Phi = \frac{1}{2}ln|1 - 2M/r| + f(t) \tag{2.7}$$

where $f(t)$ is an arbitrary function, from which the time coordinate can be redefined as

$$t_{new} = \int e^{f(t)}dt,$$

and thereby obtain the Schwarzschild line element of the form

$$ds^2 = -\left(1 - \frac{2GM}{c^2 r}\right)c^2 dt^2 + \left(1 - \frac{2GM}{c^2 r}\right)^{-1} dr^2 + r^2(d\theta^2 + sin^2\theta \ d\phi^2) \tag{2.8}$$

Now that the Schwarzschild Line element was derived from spherical symmetry arguments, we will proceed to derive the *Lagrangian* for this line element in the follwing section, from which we will conduct the analysis of massive and light-like particle geodesic motion, which will set, with foresight, the ground for a comparative study to be done in the newly obtained non-singular metric. After the discussion on geodesics is carried, the last sections in this chapter will discuss aspects related to the singularity theorem in a general space-time metric with certain features (not specific to the Schwarzschild solution), and from there lead the discussion into nothing else but *resolving these singularities*.

2.2   Geodesic Motion

The equations governing the geodesics in space-time with the line element [7]

$$ds^2 = g_{ij}\ dx^i dx^j \tag{2.9}$$

Can be derived from the Lagrangian

$$2\mathcal{L} = g_{ij}\ \frac{dx^i}{d\tau}\frac{dx^j}{d\tau} \tag{2.10}$$

where τ is some affine parameter along the geodesic. For time-like geodesics, τ may be identified with the proper time, s, of the particle describing the geodesic.

For a general spherically symmetric space-time, with $g_{00} = (g_{11})^{-1} = g(r)$, which is relevant to our problem , the Lagrangian is

$$\mathcal{L} = \frac{1}{2}\left[g(r)\dot{t}^2 - \frac{\dot{r}^2}{g(r)} - r^2\dot{\theta}^2 - (r^2 sin^2\theta)\dot{\phi}^2 \right] \tag{2.11}$$

where the dot denotes differentiation with respect to τ. The corresponding canonical momenta are

$$p_t = \frac{\partial\mathcal{L}}{\partial\dot{t}} = g(r)\dot{t}, \quad p_\phi = -\frac{\partial\mathcal{L}}{\partial\dot{\phi}} = (r^2 sin^2\theta)\dot{\phi}$$

$$p_r = -\frac{\partial\mathcal{L}}{\partial\dot{r}} = (g(r))^{-1}\dot{r}, \quad p_\theta = -\frac{\partial\mathcal{L}}{\partial\dot{\theta}} = r^2\dot{\theta}$$

The resulting Hamiltonian is

$$\mathcal{H} = p_t\dot{t} - (p_r\dot{r} + p_\theta\dot{\theta} + p_\phi\dot{\phi}) - \mathcal{L} = \mathcal{L} \tag{2.12}$$

The equality of the Hamiltonian and the Lagrangian signifies that there is no 'potential energy' in the problem: the energy is derived solely from the 'kinetic energy' as is, indeed, manifest from the expression (2.10) for the Lagrangian. The constancy of the Hamiltonian and the Lagrangian follow from this fact:

$$\mathcal{H} = \mathcal{L} = constant. \tag{2.13}$$

By rescaling the affine parameter τ, we can arrange that $2\mathcal{L}$ has the value $+1$ for time-like geodesics, and *zero* for null geodesics.
Further integrals of motion follow from the equations

$$\frac{\partial p_t}{\partial\tau} = \frac{\partial\mathcal{L}}{\partial t} = 0 \quad and \quad \frac{\partial p_\phi}{\partial\tau} = \frac{\partial\mathcal{L}}{\partial\phi} = 0 \tag{2.14}$$

Thus

$$p_t = \left(1 - \frac{2M}{r}\right)\frac{dt}{d\tau} = constant = E \tag{2.15}$$

and

$$p_\phi = r^2 sin^2(\theta)\frac{\partial\phi}{\partial\tau} = constant$$

Moreover, if we choose to asign the value $\pi/2$ to θ when $\dot\theta$ is zero, then the geodesic will be described in n invariant plane which we may distinguish by $\theta = \pi/2$. Then for p_ϕ we get

$$p_\phi = r^2\frac{\partial\phi}{\partial\tau} = constant = L \tag{2.16}$$

where L denotes the angular momentum about an axis normal to the invariant plane. With $\dot t$ and $\dot\phi$ given by equations (2.15) and (2.16), the constancy of the Lagrangian gives

$$\frac{E^2}{g(r)} - \frac{\dot r^2}{g(r)} - \frac{L^2}{r^2} = 2\mathcal{L} = +1 \quad or \quad 0 \tag{2.17}$$

depending on whether we are considering time-like or null geodesics.

2.2.1 Falling into the Black Hole

Radial Time-like Geodesics

To study the motion of a massive particle on time-like geodesics, equation (2.17) is rewritten in the form

$$\left(\frac{dr}{d\tau}\right)^2 + g(r)\left(1 + \frac{L^2}{r^2}\right) = E^2 \tag{2.18}$$

The radial geodesics of zero angular momentum will further illustrate essential features of the space-time in question. Setting $L = 0$, equation (2.18) becomes

$$\left(\frac{dr}{d\tau}\right)^2 + g(r) = E^2 \tag{2.19}$$

for a general metric function $g(r)$.

For the Schwarzschild metric function given by $g(r) = 1 - 2M/r$, we get the known expression

$$\left(\frac{dr}{d\tau}\right)^2 + \left(1 - \frac{2M}{r}\right) = E^2 \tag{2.20}$$

Isolating $-2M/r$ as the effective potential (V_{Schw}) in the problem, the graph for $V(r)$ for the energy expression (2.20) (displayed for later comparative purposes) can be shown below.
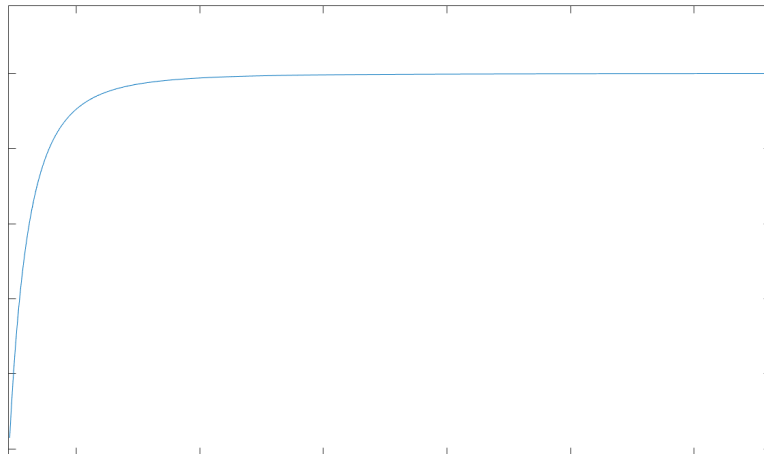
Figure 2.1: Effective potential $V(r)$ vs r for in-falling particle in Schwarzschild space-time

Plunging into the blackhole

Consider a particle plunging into the black hole, with a negative initial velocity-indicating this inward motion, starting from $r \gg 2M$, and a total energy slightly greater than the potential at that point. The particle will simply build up speed as it moves toward the $r = 0$ point, then it reaches the $r = 0$ point in finite proper-time, which we can get if we integrate (2.20), and consequently get

$$\tau = -\frac{\sqrt{2}}{3\sqrt{M}}\left(r^{3/2} - r_0^{3/2}\right) \tag{2.21}$$

with the minus sign indicating positive proper-time as r decreases from the starting point r_0 to $r = 0$. Thus, an in-falling particle reaches the center of the black hole at $r = 0$ in finite proper time.

Radial Null Geodesics

To primarily probe the space-time of the Schwarzschild geometry, we look at radial light-geodesics, where the relevant equations are Eq.(2.17) and (2.15)

$$\left(\frac{dr}{d\tau}\right) = \pm E \quad and \quad \left(1 - \frac{2M}{r}\right)\frac{dt}{d\tau} = E \tag{2.22}$$

Accordingly,

$$\frac{dr}{dt} = \pm\left(1 - \frac{2M}{r}\right) \tag{2.23}$$

which, when integrated, gives the radial light geodesics given by

$$t = \pm r \pm 2Mln\left(\frac{r}{2M} - 1\right) + constant \tag{2.24}$$

Equations (2.22) and (2.24) shows that, while the radial geodesic crosses the horizon in its own proper time without even noticing it, which we see from $r = \pm E\tau + constant$ if we integrate (2.22), it takes an infinite time-coordinate to arrive at the horizon. This is made manifest in Fig.2.2, where light cones are indicated as well. The important conclusion from this diagram is that inside the horizon region, the light cones are tilted towards the singularity at $r = 0$, indicating the *inevitability* of the singularity for any geodesic having crossed the horizon at $r = 2M$.
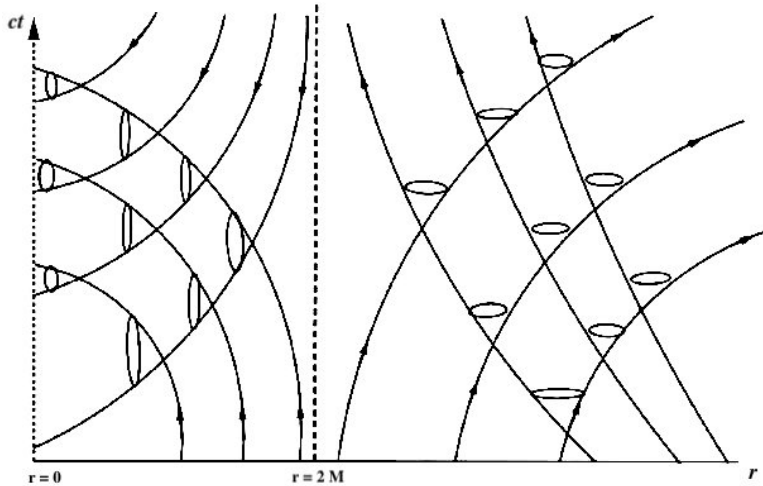
Figure 2.2: Ingoing and outgoing radial null-geodesics in the Schwarzschild coordinates

2.2.2 Motion in Schwarzschild Geometry

Particle Orbits

The time-like geodesics are once again given by Eq.(2.18)

$$\left(\frac{dr}{d\tau}\right)^2 + V(r) = E^2 \tag{2.25}$$

where the effective potential (shown in Fig.2.3) for the Schwarzschild metric is given by

$$V(r) := \left(1 - \frac{2M}{r}\right)\left(1 + \frac{L^2}{r^2}\right) \tag{2.26}$$
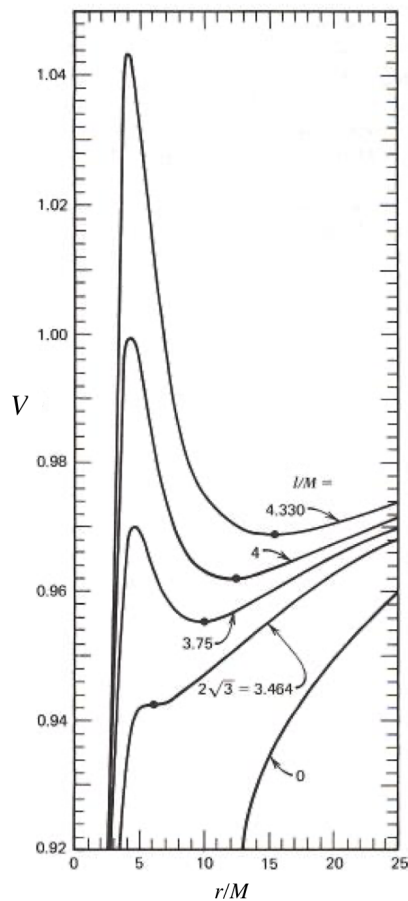
Figure 2.3: Schwarzschild Effective Potential diagram with various L [1]

10

The main conclusions about qualitative features of particle orbits are summarized below [1]:

1. Orbits with periastron at $r \gg M$ are Keplarian in form.

2. Orbits with periastron at $r < 10M$ differ markedly from Keplarian orbits.

3. For $L/M \leq 2\sqrt{3}$, any incoming particle is necessarily pulled into $r = 2M$.

4. For $2\sqrt{3} < L/M < 4$ there are bound orbits; but any particle coming in from $r = \infty$ (unbound; $E^2 \geq 1$) necessarily gets pulled into $r = 2M$.

5. For $L/M > 4$, there are bound orbits; particles coming in from $r = \infty$ with

$$E^2 < V^2_{max} \tag{2.27}$$

reach periastrons and then return to $r = \infty$; but particles from $r = \infty$ with $E^2 > V^2_{max}$ get pulled into $r = 2M$.

6. There are stable circular orbits at the minimum of the effective potential; the minimum moves inward from $r = \infty$ for $L = \infty$ to $r = 6M$ for $L/M = 2\sqrt{3}$.

7. There are unstable circular orbits at the maximum of the effective potential; the maximum moves outward from $r = 3M$ for $L = \infty$ to $r = 6M$ for $L/M - 2\sqrt{3}$. A particle in such a circular orbit, if perturbed inward, will spiral into $r = 2M$.

Photon Orbits

In the previous section, a detail was omitted for simplicity, but will become important in the discussion of orbits of zero rest-mass. The original expression of the Lagrangian given by Eq.(2.10)

$$2\mathcal{L} = g_{ij} \frac{dx^i}{d\tau} \frac{dx^j}{d\tau}$$

assumed that the rest mass of the particle is given in natural units ($\mu^2 = 1$), but now we will keep the rest mass μ^2 in the equation of the magnitude of the 4-vector of energy momentum, such that it is given by

$$g_{ij} \frac{dx^i}{d\tau} \frac{dx^j}{d\tau} = \mu^2 \tag{2.28}$$

11

and hence the Energy expression, in analogy with Eq.(2.18), can be rewritten as

$$\left(\frac{dr}{d\lambda}\right)^2 + g(r)\left(1 + \frac{\tilde{L}^2}{r^2}\right) = \tilde{E}^2 \tag{2.29}$$

where λ is an affine parameter, and E and L are given 'per unit mass' as

$$\tilde{E} = \frac{E}{\mu} \tag{2.30}$$

$$\tilde{L} = \frac{L}{\mu} \tag{2.31}$$

In the limit $\mu \to 0$, these quantities infividually go to *infinity*, but their ratio goes to a finite value, which defines the *impact parameter b*

$$\lim_{\mu \to 0} \frac{\tilde{L}}{\tilde{E}} = b \tag{2.32}$$

In this limit, Eq.(2.29) reduces to the simple form

$$\left(\frac{dr}{d\lambda}\right)^2 + B^{-2}(r) = b^{-2} \tag{2.33}$$

where $B^{-2}(r)$ defines an 'effective potential for a photon' [1]

$$B^{-2}(r) = g(r) \cdot r^{-2} \tag{2.34}$$

and the impact parameter has the the following interpretation: A ray, in order to reach the point r, must have an impact parameter

$$b \le B(r)$$

The effective potential $B^{-2}(r)$ can now be used to study qualitative features of photon orbits. For the Schwarzachild metric $g(r) = 1 - 2M/r$, the diagram is given below
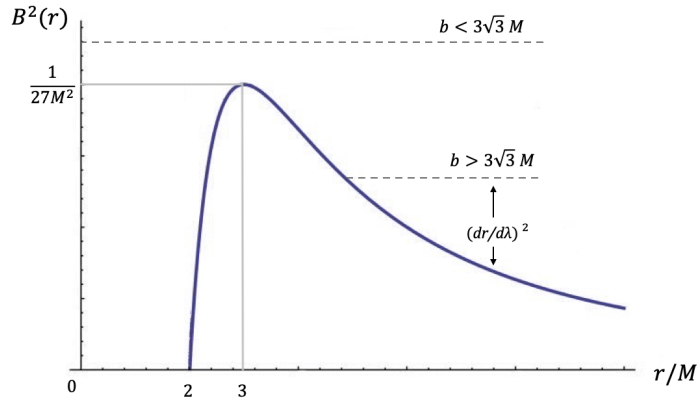
Figure 2.4: Effective Potential for a Photon in Schwarzschild Geometry

As can be deduced from the effective-potential diagram, there are three cases that can be studied [1]:

1. An in-falling photon from $r = \infty$ with $b > 3\sqrt{3}M$, is "reflected off the potential barrier, and returns to infinity.

   (a) For $b \gg 3\sqrt{3}M$, the orbit is a straight line except for a slight deflection.

   (b) For $0 < b - 3\sqrt{3}M \ll M$, the photon circles the star many times on an unstable circular orbit at $r = 3M$ before flying back to $r = \infty$

2. A photon eith $b < 3\sqrt{3}M$, falling from $r = \infty$, falls into $r = 2M$.

3. A photon emitted near $r = 2M$, escapes to infinity only if it has $b < 3\sqrt{3}M$, otherwise it reaches the barrier and falls back into $r = 2M$.

13

2.3   Causal Structure of Schwarzschild Space-time

To further study asymptotic properties of the Schwarzschild space-time, recall the line element given by Eq.(2.8)

$$ds^2 = -\Big(1 - \frac{2GM}{c^2 r}\Big)c^2 dt^2 + \Big(1 - \frac{2GM}{c^2 r}\Big)^{-1} dr^2 + r^2(d\theta^2 + sin^2\theta \; d\phi^2)$$

where
$$t \in (-\infty, \infty), \quad r \in (0, \infty), \quad \theta \in [0, \pi], \quad \phi \in [0, 2\pi) \tag{2.35}$$

The metric is singular at $r = 0$ and at $r = 2M$. To show that only $r = 0$ is a real singularity, or that any odd-ly behaving point in a metric has a real physical significance, we look at curvature invariants for this purpose, and see how they behave in different limits.

Kretschmann scalar

Because the Ricci scalar is null-valued in empty space, we will look at the *Kretchmann scalar* for the Schwarzschild metric,

$$R_{\beta\gamma\delta}R^{\beta\gamma\delta} = \frac{48M^2}{r^6} \tag{2.36}$$

which shows that the singularity at $r = 0$ is the only real singularity, because the space-time invariant does not diverge at $r = 2M$, implying it is just a coordinate singularity. This singularity indicated that the Schwarzschild coordinates (2.35) do not cover the whole space-time manifold, where there are two separated regions $r \in (0, 2M)$ and $r \in (2M, +\infty)$. This will require the use of a different set of coordinates, through which will be able to study the causal structure of the Schwarzschild space-time.

Space-time Causal Structure

We can present the Schwarzschild metric in a form which is not singular at $r = 2M$ using different coordinates, through which we can extend the exterior Schwarzschild manifold $r \in (2M, +\infty)$ beyond the Schwarzschild sphere $r = 2M$. A maximal time symmetric extension is given by the known Kruskal-Szekeres coordinates,

$$u \in (-\infty, \infty), \quad v \in (-\infty, \infty), \quad \theta \in [0, \pi], \quad \phi \in [0, 2\pi) \tag{2.37}$$

where for $r > 2M$

$$u = \pm\left(\frac{r}{2M} - 1\right)^{1/2} e^{r/4M} cosh\left(\frac{t}{4M}\right) \tag{2.38}$$

$$v = \pm\left(\frac{r}{2M} - 1\right)^{1/2} e^{r/4M} sinh\left(\frac{t}{4M}\right) \tag{2.39}$$

and for $r < 2M$

$$u = \pm\left(1 - \frac{r}{2M}\right)^{1/2} e^{r/4M} sinh\left(\frac{t}{4M}\right) \tag{2.40}$$

$$v = \pm\left(1 - \frac{r}{2M}\right)^{1/2} e^{r/4M} cosh\left(\frac{t}{4M}\right) \tag{2.41}$$

The Schwarzschild metric in these coordinates becomes

$$ds^2 = -\frac{32M^3}{r} e^{-r/2M}(-dv^2 + du^2) + r^2(d\theta^2 + sin^2\theta \, d\phi^2) \tag{2.42}$$

where $r := r(u, v)$ is defined by

$$\left(\frac{r}{2M} - 1\right) e^{r/2M} = u^2 - v^2 \tag{2.43}$$

Now we can see that the metric is regular at $r = 2M$, and the singularity at $r = 0$ is now given by $v^2 - u^2 = 1$ in the Kruskal-Szekeres coordinates.

To demonstrate the full causal structure of the Schwarzschild space-time, we map the space-time given by Eq.(2.42) and (2.37) into the corresponding conformal diagram, by applying the appropriate conformal transformation given by

$$u + v = tan\left(\frac{T + R}{2}\right), \quad v - u = tan\left(\frac{T - R}{2}\right) \tag{2.44}$$

The resulting diagram is shown in Fig.2.5, and it demonstrates causal connections between the different regions, horizons, and also the infinities and singularities of the Schwarzschild space-time.
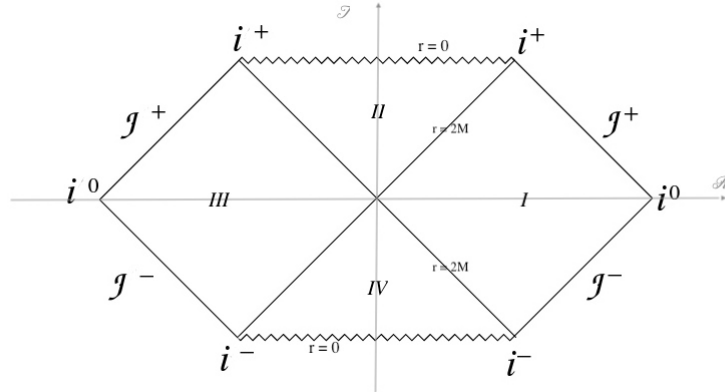
Figure 2.5: Penrose-Carter Conformal Diagram for the Schwarzschild Space-time

In obtaining the Penrose diagram, his classical definitions were used:

i^- is past time-like infinity corresponding to $t \to -\infty$ and finite r,

i^+ is past time-like infinity corresponding to $t \to +\infty$ and finite r,

i^0 is past time-like infinity corresponding to $r \to +\infty$ and finite t,

$\mathcal{J}^-$ is past time-like infinity corresponding to $t - r \to -\infty$ and finite $t + r$,

$\mathcal{J}^+$ is past time-like infinity corresponding to $t + r \to +\infty$ and finite $t - r$

Regions I and III — are asymptotically flat. They represent two identical universes, nonetheless distinct. These universes are causally disconnected.

Region II — is the Schwarzschild black hole interior. It represents an anisotropic collapsing universe of infinite spatial volume. The radial coordinate r becomes time-like in this region. So, the propagation in the black hole interior towards the singularity can be thought of as time-evolution. Particles moving along causal lines and entering the black hole interior can never escape to the outside, as they cannot move backward in time.

Region IV — is region II with the reversed direction of time. This region represents the interior of the white hole. It is an expanding anisotropic universe, which cannot be reached from the outside by causal particles. Particles moving inside of the region escape with the flow of time, inevitably. Thus, all particles in region IV in fact came out from the singularity that exists in their past.

2.4 Singularity Theorem and "The Issue of The Final State"

Now that the previous sections gave a taste of the overall techniques, attention in this discussion, which is partly borrowed from Gravitation [1], will focus on a qualitative description of the results: How does gravitational collapse end? Is the singularity at the end point of spherical collapse typical or can asymmetries remove it? That singularities are very general phenomena, and cannot be wished away, has been known since 1965, thanks to the theorems on singularities proved by Penrose, Hawking and Geroch.

Before examining the theorems on singularities, one must make precise the concept of a singularity. It is not easy, as Geroch (1968) pointed out in a long treatise on the great variety of pathologies that can arise in space-time manifolds. However, after vigorous efforts by many, Schmidt (1970) finally produced a definition that appears satisfactory. In heuristic terms, Schmidt's highly technical definition goes something like this. In a space-time manifold, consider all spacelike geodesics ("tachyon" paths), all null geodesics (photon paths), all timelike geodesics (free falling observer paths), and all timelike curves with bounded acceleration (paths along which obervers are able to move in principle). Suppose the one of these curves terminates after the lapse of finite proper length (or finite affine parameter in the null geodesic case). Suppose further that it is impossible to extend the space-time manifold beyond this termination point, for example because of the infinite curvature. The this termination point, with all adjacent termination points, is called a "singularity" (What could be more singular than the cessation of existence for the poor tachyon, photon or observer that moves along terminated curve?).

Penrose Singularity Theorem

Another concept needed in singularity theorems is that of a *trapped surface*. The concept, devised by Penrose (1965b), is motivated by a careful examination of two-dimensional spherical surfaces $(r, t) = cst$ inside the horizon of the Schwarzschild geometry. These surfaces signal the proximity of a singularity (r = 0) by this property: the light rays emitted by one of these surfaces in the direction perpendicular to the outside (that is to say the outgoing, orthogonal null) converge towards each other as they propagate; and the inward light rays perpendicular to the surface 2 also converge. Penrose gives the name of "trapped surface" to any surface closed to 2 surfaces, spherical or not, which has this property. In Schwarzschild space-time, the convergence of light rays, both outgoing and incoming, can be attributed to "the intense pull of gravity", which sucks photons into the singularity. This might also be true in asymmetric space-times is suggested by the Hawking-Penrose Theorem (1969):

A spacetime M necessarily contains incomplete, inextendable timelike or null geodesics (and is thus singular in the Schmidt sense) if, in addition to Einstein's equations, the following four conditions hold: (1) M contains no closed timelike curves (reason- able causality condition); (2) at each event in M and for each unit timelike vector $\vec{u}$, the stress-energy tensor satisfies

$$\left(T_{\alpha\beta} - \frac{1}{2}g_{\alpha\beta}T\right)y^{\alpha}u^{\beta} \geq 0 \qquad (2.45)$$

(reasonable energy condition); (3) the manifold is "general" (ie., not too highly symmetric) in the sense that every timelike or null geodesic with unit tangent $\vec{u}$ passes through at least one event where the curvature is not lined up with it in a specific way:

$$u_{[\alpha}R_{\beta]\gamma\delta[\epsilon}u_{\rho]}u^{\gamma}u^{\delta} \neq 0 \quad \text{at some point on the geodesic} \qquad (2.46)$$

(4) the manifold contains a trapped surface.

All these conditions, except the trapped surface, seem eminently reasonable for any physically realistic space-time, if one is not considering a modification of the gravitational theory at all! Note, especially, that the energy condition can be violated only if, as measured by some local observer in his proper frame, the total energy density E is negative or the principal pressures (eigenvalues of stress tensor) P_i, are so negative that

$$\sum_i P_i < -E \qquad (2.47)$$

"The issue of the final state"

If, as one suspects today, the singularities are of a very physical, infinite-curvature type, then one must face up to John Wheeler's (1964a) "issue of the final state" in its most raw and disturbing form. Wheeler, when faced with this issue, argues that infinite-curvature singularities signal a breakdown in classical general relativity–a breakdown forced by the onset of quantum gravitational phenomena. Whether quantization of gravity will actually save space-time from such singularities one cannot know until the "fiery marriage of general relativity with quantum physics has been consummated.

An intro to "classically resolving singularities"

The last passage ended with an optimistic note on a way to resolve the diverging properties of singularities through a suggested merger of gravity and quantum physics. As mentioned earlier, the progress along this line of research has been relatively modest inspite of the enormous efforts devoted to the problem, and while the "quantum resolution" of singularities remains rather obscure, the work that will be discussed in the following chapter will present a classical way to resolve such singularities, by introducing a modification to Einstein's gravity theory at very high curvatures, all the while protecting the results obtained for a gravitational field of a massive body from Einstein's theory which celebrated many observational triumphs, at the limit within reach.

Chapter 3

Non-Singular Solution in Mimetic Gravity

3.1 Mimetic Gravity

Metric with scalar field

Einstein's gravity is distinguished by the fact that it has equations which are only second order. Without altering this property, "mimetic gravity" which was introduced in a paper in 2013 by Chamseddine and Mukhanov [8], proposed a way to modify gravity theory by the reshuffling of the degrees of freedom of the metric itself. Starting by re-parametrizing the physical metric $g_{\mu\nu}$ in the form:

$$g_{\mu\nu} = h_{\mu\nu} \ h^{\alpha\beta}\varphi_{,\alpha}\varphi_{,\beta} \qquad (3.1)$$

in terms of the auxiliary metric $h_{\mu\nu}$ and a scalar field φ, called the mimetic field. The physical metric is invariant under Weyl transformations of $h_{\mu\nu}$, and the mimetic field represents the conformal degree of freedom of gravity, where φ by definition satisfies

$$g_{\mu\nu} \ \varphi_{,\mu} \ \varphi_{,\nu} = 1 \qquad (3.2)$$

and the nature of the mimetic field can be introduced by adding the above condition on φ as a constraint to the gravity action, which in turn takes the following general form

$$S \ = \ \frac{1}{16\pi} \ \int d^4x \ \sqrt{-g} \ \left(-\mathcal{L}\left[g_{\mu\nu}, \varphi\right] + \ \lambda \left(g_{\mu\nu}\partial_\mu\varphi \ \partial_\nu\varphi - 1\right)\right) \qquad (3.3)$$

where λ is a Lagrange multiplier. The constraint (3.2) could also be obtained as a consequence of 3D volume quantization in noncommutative geometry [9], [10].

3.2 Theory with Asymptotic Freedom

General Lagrangian

By inserting the Einstein-Hilbert Lagrangian $L = R[g_{\mu\nu}]$, the authors were able to reproduce just the standard GR with an additional contribution of mimetic matter in [8],[11]. However, in the work from which this study will follow [2], the authors used the mimetic field to implement in a covariant way the idea of a running gravitational and cosmological constant by introducing into the action a Lagrangian given by

$$L = f[\varphi] R[g_{\mu\nu}] + 2\Lambda[\varphi] \tag{3.4}$$

where f is the "inverse gravitational constant" and Λ is the "cosmological constant", and they will depend on ϕ and its derivatives in a way to be determined.

Extrinsic curvature measure

Considering a synchronous coordinate system

$$ds^2 = dt^2 - \gamma_{ij}\left(t, x^i\right) dx^i dx^j \tag{3.5}$$

where $t = \phi$ can be used as the time-coordinate, it can be seen that including a simple φ dependence of f and Λ would resemble the presence of a time-dependent background.

As will be seen, the second covariant derivatives of ϕ, will represent measures of the curvature related to the conformal degree of freedom of the gravitational field. Evaluating the second covariant derivative of ϕ

$$-\phi_{;ab} = \kappa_{ab} = \frac{1}{2}\frac{\partial}{\partial t}\gamma_{ab}$$

gives the extrinsic curvature of the slices of constant ϕ, where $\phi_{;0\alpha} = 0$. In this synchronous slicing given by ϕ, the Ricci scalar can be expanded as

$$-R = 2\dot{\kappa} + \kappa^2 + \kappa_b^a \kappa_a^b + {}^3R, \tag{3.6}$$

where dot denotes t-derivatives, $\kappa_b^a = \gamma^{ac}\kappa_{cb}$, ${}^3R$ is the 3-curvature of the spatial slices and

$$\kappa := \gamma^{ab}\kappa_{ab} = g^{\alpha\beta}\phi_{;\alpha\beta} = \Box\phi$$

is the trace of extrinsic curvature.

Theory free of high-order derivatives

From expression for Ricci scalar in Eq.(3.6), it becomes clear why the Einstein equation is second-order: the second derivatives of the metric appear linearly in R and hence contribute as total-derivatives to the action only. So to introduce a curvature-dependence into the gravitational constant and protect this property is through $f[\phi] = f(\Box\phi)$. In this case, the full Ricci scalar term with the running gravitational constant can be expanded in relevant quantities as

$$-f(\Box\phi)R = 2\dot{F}(\kappa) + f(\kappa)\left(\kappa^2 + \kappa_b^a\kappa_a^b + {}^3R\right) \tag{3.7}$$

where $f(\kappa) = F'(\kappa) \equiv \partial F/\partial\kappa$. Up to a total derivative, this Lagrangian still contains only first time-derivatives of the metric, and it can be expected that the modified Einstein equation of such a theory to be second-order in time. While it is not allowed to use $\Box\phi = \kappa$ and impose gauge conditions in the action before variation, this statement can be explicitly verified. The theory defined by

$$\mathcal{L} = f(\Box\phi)R + 2\Lambda(\Box\phi) \tag{3.8}$$

which was studied in [12], it was shown to be free of higher time-derivatives in the synchronous frame. However, in the general case where spatial flatness is not guaranteed, higher spatial and mixed derivatives will appear. These terms can be traced back to the presence of $f(\Box\phi)$ in front of ${}^3R$ in Eq.(3.7), we can use ϕ to expand this term in a covariantly as

$$\widetilde{R} = 2\phi^{,\mu}\phi^{,\nu}G_{\mu\nu} - (\Box\phi)^2 + \phi^{;\mu\nu}\phi_{;\mu\nu} \doteq {}^3R,$$

where $G_{\mu\nu}$ is the Einstein tensor and the last equality holds under the condition that the constraint in Eq.(3.2) is satisfied. So, by subtracting the term which was involuntarily added, the theory defined by

$$\mathcal{L} = f(\Box\phi)R + (f(\Box\phi) - 1)\widetilde{R} + 2\Lambda(\Box\phi)$$

will be free of higher derivatives. Hence the second summand was added on the same basis which made Einstein gravity unique.

In the context of a theory defined by the Lagrangian in Eq.(3.8), it is natural to realize the concept of limiting curvature (as in [5],[13],[14]) by limiting the measure of curvature provided by $\Box\phi$. Motivated by the analysis of the anisotropic sector made in [12], the concept of "asymptotic freedom" of gravity is especially important in relation to modifications where such a limiting-curvature

is implemented by a vanishing of the gravitational constant at some limiting value $\Box\phi = \kappa_0$, which is a free parameter of the theory and can be chosen well below the Planckian curvature.

3.3   Action and equations of motion

This section with further show developments of the theory in [2] defined by the action

$$S = \frac{1}{16\pi} \int \mathrm{d}^4 x \sqrt{-g}\left(-\mathcal{L} + \lambda\left(g^{\mu\nu}\phi_{,\mu}\phi_{,\nu} - 1\right)\right),\tag{3.9}$$

with the general extended Lagrangian

$$\mathcal{L} = f(\Box\phi)R + (f(\Box\phi) - 1)\widetilde{R} + 2\Lambda(\Box\phi) + h(\widetilde{R})\tag{3.10}$$

and

$$\widetilde{R} = 2\phi^{,\mu}\phi^{,\nu}G_{\mu\nu} - (\Box\phi)^2 + \phi^{;\mu\nu}\phi_{;\mu\nu}.\tag{3.11}$$

Once again, the action contains two free functions f and Λ of $\Box\phi$, representing the inverse running gravitational constant $G(\Box\phi)^{-1}$ and cosmological constant $\bar{\Lambda}(\Box\phi)$, respectively. The spatial-curvature dependent potential $h(\widetilde{R})$ was included for generality in the derivation, but won't be needed in a spatially-flat case that the authors solve for later. In the following, Planck units will be used such that G is set to be $G(\Box\phi = 0) = G_0 = 1$, such that $f(\Box\phi = 0) = 1$.

The modified Einstein Equations are hence obtained below, by the variation of the action with respect to the metric $g_{\mu\nu}$

$$(1 - h')R_{\mu\nu} - \left(\tfrac{1}{2}\mathcal{L} + (\tilde{Z}\phi^{,\alpha})_{;\alpha} + \Box h'\right)g_{\mu\nu} + \left(\phi_{,\mu}\phi_{,\nu}\tilde{f}^{,\alpha} - \phi_{;\mu\nu}\tilde{f}\phi^{,\alpha}\right)_{;\alpha}$$

$$+ 2\tilde{f}\phi^{,\alpha}\phi_{(,\mu}R_{\nu)\alpha} + 2\phi_{(,\mu}\tilde{Z}_{,\nu)} + h'_{;\mu\nu} = (\lambda + \tilde{f}R)\phi_{,\mu}\phi_{,\nu} + 8\pi T^{(\mathrm{m})}_{\mu\nu},\tag{3.12}$$

where

$$\tilde{f} := f - 1 + h', \qquad Z := \tfrac{1}{2}f'\left((\Box\phi)^2 + \phi^{;\mu\nu}\phi_{;\mu\nu}\right) - \Lambda', \qquad \tilde{Z} := Z - \phi^{,\alpha}h'_{,\alpha},$$

$f' := \mathrm{d}f/\mathrm{d}\Box\phi$, $\Lambda' := \mathrm{d}\Lambda/\mathrm{d}\Box\phi$, $h' := \mathrm{d}h/\mathrm{d}\widetilde{R}$ and $T^{(\mathrm{m})}_{\mu\nu} = \frac{2}{\sqrt{-g}}\frac{\delta S^{\mathrm{m}}}{\delta g^{\mu\nu}}$ is the matter energy momentum tensor.

The evolution of the mimetic field is already completely determined by the constraint (3.2), which we obtain from variation with respect to the Lagrange multiplier. The equation obtained by varying (3.9) with respect to ϕ hence can only return the favor and provide a condition to determine λ. Conveniently written in terms of the quantity

$$\Xi := \lambda + \tilde{f}\left(R - R_{\mu\nu}\phi^{,\mu}\phi^{,\nu}\right) - \Box f - \phi^{,\mu}Z_{,\mu} - \phi^{,\mu}h'_{,\mu}\Box\phi, \qquad (3.13)$$

this "equation of motion" of ϕ reads

$$(\Xi\,\phi^{,\nu})_{;\nu} = \left[(f - h')^{,\mu}\phi^{;\nu}_\mu + Z^{,\nu} - \phi^{,\nu}\phi^{,\mu}Z_{,\mu} + \Box\phi\left(h'^{,\nu} - \phi^{,\nu}\phi^{,\mu}h'_{,\mu}\right)\right.$$
$$\left. + \ \tilde{f}\left(R^{\mu\nu}\phi_{,\mu} - R^{\alpha\beta}\phi_{,\alpha}\phi_{,\beta}\phi^{,\nu}\right)\right]_{;\nu}. \qquad (3.14)$$

In the synchronous frame the right hand side turns out to be just the 3-divergence of a 3-vector (denoted by $X^a_{|a}$) and we find the solution

$$\Xi = \frac{1}{\sqrt{\gamma}}\int \mathrm{d}t\sqrt{\gamma}\left(\kappa^a_b f^{,b} + Z^{,a} + \tilde{f}R^a_0 + \kappa h'^{,a} - \kappa^a_b h'^{,b}\right)_{|a}. \qquad (3.15)$$

Einstein Equations in the synchronous frame

Temporal-components — The modified Einstein equation in Eq.(3.12) take a simple form when evaluated in the synchronous frame $t = \phi$, and the $0-0$ component of the modified Einstein equation becomes

$$\frac{1}{3}\left(f - 2\kappa f'\right)\kappa^2 - \Lambda + \kappa\Lambda' - \frac{1}{2}\left(f + \kappa f'\right)\tilde{\kappa}^a_b\tilde{\kappa}^b_a = \frac{1}{2}\left(h - {}^3R\right) + \Xi + 8\pi T^{(\mathrm{m})}_{00}, \quad (3.16)$$

where $\tilde{\kappa}^a_b := \kappa^a_b - \frac{1}{3}\kappa\delta^a_b$ is the traceless part of the extrinsic curvature.

Dynamical conformal dof — Inserting the solution (3.15) for Ξ, and by taking another time-derivative of the temporal-modified Eintein Equaiton (3.16), a differential equation containing second time derivatives of the metric is obtained. This shows that in mimetic gravity the conformal degree of freedom of the gravitational field becomes dynamical.

Spatial-components — The spatial components of the modified Einstein equation in (3.12) with one raised index read

$$-\frac{1}{\sqrt{\gamma}} \, \partial_t \left(\sqrt{\gamma} \, (f\kappa_b^a + Z\delta_b^a) \right) - \tfrac{1}{2}\mathcal{L} \, \delta_b^a = S_b^a + 8\pi T^{(\mathrm{m})a}{}_b, \tag{3.17}$$

where

$$S_b^a := (1 - h')^3 R_b^a + h'{}^{|a}_{\ b} - \Delta h' \delta_b^a \tag{3.18}$$

contains spatial curvature terms. Subtracting one third of the (spatial) trace of this equation, the following is obtained

$$-\frac{1}{\sqrt{\gamma}} \, \partial_t \left(\sqrt{\gamma} \, f \, \tilde{\kappa}_b^a \right) = \tilde{S}_b^a + 8\pi \tilde{T}^{(\mathrm{m})a}{}_b \tag{3.19}$$

where the right hand side consists of the traceless parts of S_b^a and $T^{(\mathrm{m})a}{}_b$. Hence, the spatial-components of the modified Einstein equation are second-order in time.

Mixed-components — The mixed-components of the modified Einstein equation (3.12) hence are

$$f R_{0a} + Z_{,a} + \kappa_a^b f_{,b} = 8\pi T^{(\mathrm{m})}_{0a}. \tag{3.20}$$

Just like in standard General Relativity, these equations contain only first time-derivatives of the metric and can be thought of as a constraint that needs to be satisfied on an initial hypersurface $\phi = \phi_\mathrm{i}$ and then continues to hold by virtue of validity of the other components of the modified Einstein equation. Nonetheless, h does not appear in the mixed equations. Moreover, the mixed components equation (3.20) can simplify (3.15) to

$$\Xi = \tfrac{1}{\sqrt{\gamma}} \int \mathrm{d}t \sqrt{\gamma} \left(T^{(\mathrm{m})a}{}_0 - (1 - h')R_0^a + \kappa h'^{,a} - \kappa_b^a h'^{,b} \right)_{|a}. \tag{3.21}$$

Now, requiring

$$f = 1 + \mathcal{O}\left(\kappa^2\right), \quad \Lambda = \mathcal{O}\left(\kappa^4\right), \quad h = \mathcal{O}\left(\widetilde{R}^2\right),$$

then, in the limit of low curvatures, the equations for the components of the modified Einstein equation (3.16), (3.17) and (3.20) are just the components of the usual Einstein equation with a contribution of mimetic matter, given by the constant of integration in Ξ.

3.4 Modified Black Hole

3.4.1 Black hole in synchronous coordinates

In GR the metric of a non-rotating, eternal black hole in the synchronous Lemaître coordinates [15] is given by

$$ds^2 = dT^2 - (x/x_+)^{-2/3} dR^2 - (x/x_+)^{4/3} r_g^2 d\Omega^2, \tag{3.22}$$

where $x = R - T$, and $r_g = 2M$. These coordinates are regular at the horizon

$$x = x_+ := \frac{4}{3}M,$$

and the region $x > 0$ covers both interior and exterior of the Schwarzschild black hole. For comoving observers with $R, \vartheta, \varphi = const.$, T represents 'proper time'. In the Schwarzschild radial coordinate $r = r_g \left(x/x_+\right)^{2/3}$ the paths followed by these synchronous observers correspond to radially infalling geodesics. They start from rest at $r \to \infty$ at proper time $T \to -\infty$ and reach the singularity at $r = 0$ at the finite proper time $T = R$.

Spatial flatness in synchronous frame — To see the way in which the BH metric in Eq.(3.22) is modified in the theory with the action in Eq.(3.9), the following ansatz is considered in the synchronous coordinates (3.5) provided by $T = \phi$

$$ds^2 = dT^2 - a^2(x) dR^2 - b^2(x) d\Omega^2, \tag{3.23}$$

where the functions a and b still depend only on $x = R - T$. The transformation to Schwarzschild coordinates t and r is given by

$$t = T - \int dx \frac{a^2}{1 - a^2}, \qquad r = b(R - T), \tag{3.24}$$

which brings the metric to the form

$$ds^2 = (1 - a^2)dt^2 - \frac{a^2}{b'^{\,2}(1 - a^2)}dr^2 - r^2 d\Omega^2. \tag{3.25}$$

The dependence of a and b' on r has to be found by inverting

$$r = b(x) \tag{3.26}$$

The spatial metric determinant of ansatz in Eq.(3.23) is

$$\gamma = a^2 b^4 \sin^2 \vartheta =: u^2(x) \sin^2 \vartheta,$$

and the non-vanishing components of the extrinsic curvature are the following

$$\kappa_R^R = \frac{\dot{a}}{a} = -\frac{a'}{a}, \qquad \kappa_\vartheta^\vartheta = \kappa_\varphi^\varphi = \frac{\dot{b}}{b} = -\frac{b'}{b},$$

where the prime denotes x-derivatives.

The spatial Ricci curvature components for the class of metrics (3.23) are given by

$$^3R_R^R = R_T^T = 2\left(\gamma^{RR}\left(\kappa_\vartheta^\vartheta\right)^2 - \gamma^{\vartheta\vartheta} + {}^3R_\vartheta^\vartheta\right),\tag{3.27}$$

$$^3R_\vartheta^\vartheta = {}^3R_\varphi^\varphi = \frac{1}{2\kappa_\vartheta^\vartheta}\left(\gamma^{RR}\left(\kappa_\vartheta^\vartheta\right)^2 - \gamma^{\vartheta\vartheta}\right)' - 2\left(\gamma^{RR}\left(\kappa_\vartheta^\vartheta\right)^2 - \gamma^{\vartheta\vartheta}\right).\tag{3.28}$$

The condition for spatial flatness hence amounts to the following equation

$$\gamma^{RR}\left(\kappa_\vartheta^\vartheta\right)^2 - \gamma^{\vartheta\vartheta} = 0 \qquad \Leftrightarrow \quad a^2 = b'^{\,2}.\tag{3.29}$$

In this case, the metric in Schwarzschild coordinates takes the form

$$\mathrm{d}s^2 = (1 - a^2)\mathrm{d}t^2 - \frac{\mathrm{d}r^2}{(1 - a^2)} - r^2\mathrm{d}\Omega^2,\tag{3.30}$$

and it can be seen that the Schwarzschild metric (3.22) is spatially flat in Lemaître coordinates.

Killing Vector Field — In the direction of the vector field

$$k^\mu\frac{\partial}{\partial x^\mu} := \frac{\partial}{\partial R} + \frac{\partial}{\partial T} = \frac{\partial}{\partial t}\tag{3.31}$$

the Lie derivative of (3.23) vanishes. So k^μ is a Killing vector field its norm given by

$$k^\mu k_\mu = 1 - a^2(x).$$

It follows that a Killing horizon occurs wherever $a^2(x) = 1$. In analogy with synchronous BH metric (3.22), denote the largest value of x where this happens, i.e. the most exterior horizon, by x_+. The surface gravity g_s can be calculated, for this Killing horizon, which is defined by the equation [16]

$$k^\nu_{;\mu}k^\mu = g_s\,k^\nu,\tag{3.32}$$

evaluated at the horizon. It can be hence shown that it is related to the extrinsic-curvature of the synchronous-slices by

$$g_s = \kappa_R^R(x_+) = -a'(x_+).\tag{3.33}$$

3.4.2   Modified Einstein equations

Considering for simplicity the theory where $h = 0$, in the following section, we show how the authors derive the modified Einstein equation for the ansatz metric of the form (3.23). By virtue of the fact that all relevant quantities depend on R and T only through the quantity $x = R - T$, one can replace $\partial_T = -\partial_R$ and

27

reduce partial differential-equations to ordinary differential-equations. For example, for the vacuum case at hand (3.21) yields

$$\Xi = -\frac{1}{\sqrt{\gamma}} \int dT\, \partial_R \left(\sqrt{\gamma} R_T^R \right) = R_T^R = {}^3R_R^R,$$

where the constant of integration is set to zero to be consistent with the asymptotic exterior vacuum solution in Eq.(3.22). Hence the temporal modified Einstein equation (3.16) becomes

$$\frac{1}{3} \left(f - 2\kappa f' \right) \kappa^2 - \Lambda + \kappa \Lambda' - \frac{1}{2} \left(f + \kappa f' \right) \tilde{\kappa}_b^a \tilde{\kappa}_a^b = \gamma^{RR} \left(\kappa_\vartheta^\vartheta \right)^2 - \gamma^{\vartheta\vartheta}. \tag{3.34}$$

The trace subtracted spatial equations (3.19) read

$$\frac{1}{u} \left(u f \tilde{\kappa}_b^a \right)' = {}^3R_b^a - \frac{1}{3} {}^3R \delta_b^a. \tag{3.35}$$

By spherical symmetry and tracelessness they contribute only one independent equation. Subtracting the $\vartheta - \vartheta$ equation from the $R - R$ equation and inserting (3.27), (3.28) it can be written as

$$\frac{1}{u} \left(u f \left(\frac{b'}{b} - \frac{a'}{a} \right) \right)' = \frac{1}{2\kappa_\vartheta^\vartheta} \left(\gamma^{RR} (\kappa_\vartheta^\vartheta)^2 - \gamma^{\vartheta\vartheta} \right)'. \tag{3.36}$$

For the Schwarzschild solution (3.22) it holds that $\kappa = -1/x$. Hence, for large mass black holes with

$$M \gg \frac{1}{\kappa_0} \tag{3.37}$$

the extrinsic curvature at the horizon $x = x_+ \approx 4M/3$ is much lower than the limiting curvature scale κ_0 and it can still be expected that the exterior solution is given by (3.22) and modifications to restrict themselves to the interior region. As it was shown before, the Schwarzschild solution (3.22) is spatially-flat in the given slicing. If one assumes that the spatial-curvature will remain negligible also for some range of x after the modification has taken over. In fact, it will be shown that the linear contribution of spatial curvature is irrelevant for the region close to the horizon even in the case $M \sim \kappa_0^{-1}$. In this spatial flatness approximation, Eq.(3.35) is easily integrated and yields

$$\tilde{\kappa}_R^R = \frac{2M}{fu}, \qquad \tilde{\kappa}_\vartheta^\vartheta = -\frac{M}{fu}, \tag{3.38}$$

where the constants of integration have been fixed to match the Schwarzschild solution in the limit $x \to \infty$. Accordingly, the simplified temporal modified Einstein equation (3.34) becomes

$$\frac{\kappa^2 \left(f - 2\kappa f' \right) - 3 \left(\Lambda - \kappa \Lambda' \right)}{f + \kappa f'} = \left(\frac{3M}{fu} \right)^2, \tag{3.39}$$

Eq. (3.38) can be integrated again to obtain the solutions for $a(x)$ and $b(x)$ as

$$a = u^{1/3} \left(\frac{2}{3} \kappa_0 e^H \right)^{2/3}, \qquad b = u^{1/3} \left(\frac{2}{3} \kappa_0 e^H \right)^{-1/3}, \qquad (3.40)$$

where the pre-factors have been chosen for dimensionality and later convenience and

$$H := \int \mathrm{d}T \, \frac{3M}{fu}. \qquad (3.41)$$

3.4.3   A Spatially Flat Exact (Implicit) Solution

Consider the asymptotically free modification given by

$$f(\kappa) = \frac{1 + 3 \left(\kappa/\kappa_0 \right)^2}{\left(1 + \left(\kappa/\kappa_0 \right)^2 \right) \left(1 - \left(\kappa/\kappa_0 \right)^2 \right)^2} \qquad (3.42)$$

$$\Lambda(\kappa) = \kappa^2 \left(\frac{\frac{4}{3} \left(\kappa/\kappa_0 \right)^2}{\left(1 - \left(\kappa/\kappa_0 \right)^2 \right)^2} - \frac{1 + 2 \left(\kappa/\kappa_0 \right)^2}{1 + 4 \left(\kappa/\kappa_0 \right)^2 + 3 \left(\kappa/\kappa_0 \right)^4} \right)$$
$$- \frac{\kappa_0}{6} \kappa \left(\arctan \frac{\kappa}{\kappa_0} - 3\sqrt{3} \arctan \left(\sqrt{3} \frac{\kappa}{\kappa_0} \right) + 2 \operatorname{arctanh} \frac{\kappa}{\kappa_0} \right) \qquad (3.43)$$

With this choice, the temporal equation (3.39) becomes

$$\frac{\kappa^2}{\left(1 - \left(\kappa/\kappa_0 \right)^4 \right)^2} = \left(\frac{3M}{u} \right)^2. \qquad (3.44)$$

Taking the time derivative of the logarithm of this equation one finds that

$$\dot{\kappa} = -\kappa^2 \frac{1 - \left(\kappa/\kappa_0 \right)^4}{1 + 3 \left(\kappa/\kappa_0 \right)^4}, \qquad (3.45)$$

which has the implicit solution

$$-\kappa_0 x = \frac{\kappa_0}{\kappa} - 2 \operatorname{atanh} \frac{\kappa}{\kappa_0} + 2 \arctan \frac{\kappa}{\kappa_0}. \qquad (3.46)$$

Evaluating (3.41) as an integral over κ yields

$$H(\kappa) = \ln \left(- \left(\kappa/\kappa_0 \right) \frac{1 + \left(\kappa/\kappa_0 \right)^2}{1 + 3 \left(\kappa/\kappa_0 \right)^2} \right), \qquad (3.47)$$

where the constant of integration was fixed to match the Schwarzschild solution. It follows that

$$\frac{a}{b} = \frac{2}{3}\kappa_0 e^H = \frac{2}{3}\left(-\kappa\,\frac{1+(\kappa/\kappa_0)^2}{1+3\,(\kappa/\kappa_0)^2}\right) = -\frac{1}{3}\left(\kappa - \frac{3M}{fu}\right) = \left|\kappa_\vartheta^\vartheta\right|, \qquad (3.48)$$

which shows that this solution is spatially flat and hence an exact solution of the full modified Einstein equation.

The implicit solutions for a and b are given by

$$a^3(\kappa) = \frac{4M}{3}|\kappa|(1-(\kappa/\kappa_0)^4)\left(\frac{1+(\kappa/\kappa_0)^2}{1+3(\kappa/\kappa_0)^2}\right)^2 \qquad (3.49)$$

$$b^3(\kappa) = \frac{9M}{2\kappa^2}(1-(\kappa/\kappa_0)^2)(1+3(\kappa/\kappa_0)^2) \qquad (3.50)$$

where a assumes its extremum value at $\kappa = \kappa_* = -\kappa_0\sqrt{5}$, and the location of this extremum in Schwarzschild r-coordinate is given by

$$r_* = b\left(\kappa_*\right) = (144M/5\kappa_0^2)^{1/3} \qquad (3.51)$$

Asymptotic limits in Schwarzschild coordinates

Transforming the metric into Schwarzschild coordinates, and by virtue of spatial flatness, the metric takes the form

$$ds^2 = \left(1-a^2\right)dt^2 - \frac{dr^2}{(1-a^2)} - r^2 d\Omega^2 \qquad (3.52)$$

The asymptotic limits of the metric functions are discussed below.

Limit at $r \to \infty$ — Far away from the black hole, in the limit $r \to \infty$, where $(\kappa/\kappa_0)^2 \ll 1$, the expansion takes the form

$$1-a^2 = 1 - \frac{2M}{r}\left[1 - \frac{5}{16}\left(\frac{r_*}{r}\right)^3 + \mathcal{O}\left(\left(\frac{r_*}{r}\right)^6\right)\right] \qquad (3.53)$$

It follows that the location of the outer horizon of a large mass black hole is given by

$$r_+ = 2M \left[1 - \frac{729}{6250} \left(\frac{M_{min}}{M} \right)^2 + \mathcal{O}\left(\left(\frac{M_{min}}{M} \right)^4 \right) \right] \tag{3.54}$$

Limit at $r \to 0$ — Close to the singularity, where limiting curvature $\kappa^2 \to \kappa_0{}^2$, the expansion is given by

$$1 - a^2 = 1 - (\zeta r)^2 \left[1 - \frac{4}{5} \left(\frac{r}{r_*} \right)^3 + \mathcal{O}\left(\left(\frac{r}{r_*} \right)^6 \right) \right] \tag{3.55}$$

where $\zeta = \kappa_0/3$ and the inner horizon occurs at

$$r_- = \zeta^{-1} \left[1 - \frac{27\sqrt{5}}{1600} \frac{M}{M_{min}} + \mathcal{O}\left(\left(\frac{M}{M_{min}} \right)^2 \right) \right] \tag{3.56}$$

Limit at $r \sim r_*$ — While both asymptotes fail to describe the region between the horizons, it can be found by expanding the solution around the maximum of a at r_*

$$1 - a^2 = 1 - \left(\frac{M}{M_{min}} \right)^{\frac{2}{3}} \left(1 - \frac{10}{7} (1 - r/r_*)^2 \right) \tag{3.57}$$

For the minimal Black Hole $M = M_{min}$, the inner and outer horizons coincide at $r_* = r_- = r_+$, and the metric close to this single horizon is given by

$$1 - a^2 \approx \frac{10}{7} (1 - r/r_*)^2 \tag{3.58}$$

Chapter 4

The Non-Singular Black Hole: A Study

4.1 Metric in Schwarzschild Coordinates

To aid our intuition, the plot of the metric function $g(r) := (1-a^2)$ in Schwarzschild r-coordinate is provided in Fig 4.1 below.
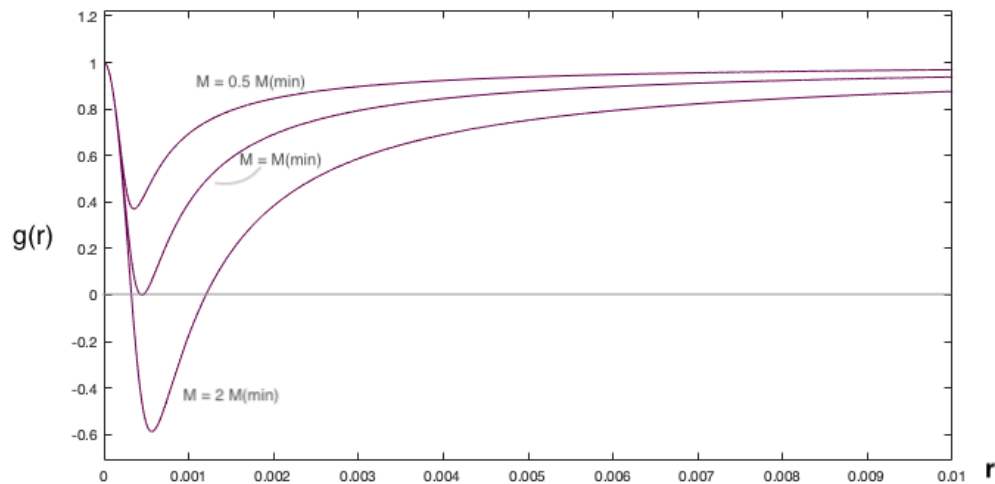

Figure 4.1: Metric function plot for $M > M_{min}$, $M = M_{min}$, and $M < M_{min}$

On the lines of Numerical vs Analytic approach

While we don't have an exact expression for the metric function in Schwarzschild r-coordinate, it was impossible to find a concise analytic expression that serves as a good fit at the horizons (when they exist) and the at the minimum, without elongating the expression to a point where it will be difficult to handle such an equation without expanding around certain points. As this just overrides the purpose of obtaining an expression to be used later in computing geodesics, the approach to studying the properties of this NSBH solution will be mixed between using numerical methods to obtain exact graphs for quantities under study, and working analytically through asymptotic limits provided in Sec.3.4.3, to give a quantitative argument when needed.

This said, the plots in Fig.4.1 are obtained by first numerically reparametrizing $a(\kappa)$ in r-coordinate, aka plotting the expression of $a(\kappa)$ vs $b(\kappa)$ given in Eq.(3.50), which is identified as the radial component in Schwarzschild coords in Eq.(3.26), then $a(r)$ is conveniently used to plot $g(r) = 1 - a^2(r)$ now in r.

On the properties of the metric function $g(r)$

This metric function describes a Schwarzschild-de Sitter smooth transition that captures the general behavior of our metric in study.

For a large blackhole with $M > M_{min}$, the metric admits two coordinate singularities in Schwarzschild coordinates, a Schwzarzschild horizon at r_+, and a de Sitter horizon at r_-. For a mininmal blackhole with $M = M_{min}$, as mentioned earlier, these two horizons coincide at $r = r_+ = r_-$. The structure with $M < M_{min}$ admits no horizons, and has a de Sitter core instead of a naked singularity at its center.

4.2   Penrose-Hawking Theorem

This is a brief section dedicated to mention the simple and obvious reason why the Penrose and Hawking Theorem is *not* valid in the scenario we are considering, and it is quoted below

Einstein's equations do NOT hold as κ approaches its limiting value, and they are hence modified as given by Eq.(3.12)

Hence, the non-singular solution given by expressions (3.49) and (3.50) that enter the metric is does not hold any contradiction with the singularity theorem. Proofs showing the regularity of the curvature invariants as we approach the point of 'singularity' namely $r = 0$, finite time needed to reach it, and geodesic completeness of the space-time will be further discussed.

Geodesic Completeness

For completeness, in [2], the authors provide an argument with a sufficient (but not necessary) condition for causal geodesic completeness of a metric of the form (3.5).

4.3   Curvature Invariants

The first test to whether we obtain a regular behavior of the metric, and which shows that problematic points in the metric, the zero points in the metric indicating the presence of horizons for instance, are nothing but a coordinate artifacts, is to obtain an expression for curvature scalars and see how they behave, taking different limits.

The Kretschmann Scalar

Just like before, we will see how $R^{\alpha\beta\gamma\delta}R_{\alpha\beta\gamma\delta}$ behaves at different limits, and it will give us a pretty good indication of how well a curvature scalar in our space-time behaves.

Here we can use the asymptotic expression of the metric given by equations (3.55),(3.57), and (3.53), and see in sections their separate behavior, keeping in mind the limit near $r = 0$ is the relevant expression.

The Riemann squared expressions for the three regions are hence

for $r \to \infty$

$$R^{\alpha\beta\gamma\delta}R_{\alpha\beta\gamma\delta} = \frac{3M^2}{16r^{12}}\left(256r^6 - 800r^3r_*^3 + 975r_*^6\right) \tag{4.1}$$

for $r \sim r_*$

$$R^{\alpha\beta\gamma\delta}R_{\alpha\beta\gamma\delta} = 4\left(\frac{M}{M_{min}}\right)^{4/3} \cdot \frac{\left(600r^4 - 1200r^3r_* + 860r^2r_* - 120rr_*^3 + 9r_*^4\right)}{49r^4r_*^4}$$

$$\tag{4.2}$$

for $r \to 0$

$$R^{\alpha\beta\gamma\delta}R_{\alpha\beta\gamma\delta} = \frac{24c^4}{25r_*^6}\left(336r^6 - 140r^3r_*^3 + 25r_*^6\right) \tag{4.3}$$

We immediately see from expression (4.3) that as $r \to 0$, $R^{\alpha\beta\gamma\delta}R_{\alpha\beta\gamma\delta}$ approaches a limiting value $24c^4$, where $c = \kappa_0/3$, and κ is the free parameter which is the limiting curvature in the theory. Therefore we don't have any diverging curvature near the singularity. To confirm the regularity of the curvature invariant for all r, we can look at the graphical plot of the Riemann squared that is obtained numerically for the metric function $g(r) = 1 - a^2(r)$, which is originally parametrized in κ.

The graph for $R^{\alpha\beta\gamma\delta}R_{\alpha\beta\gamma\delta}$ obtained numerically is shown below in Fig.4.2. The plot confirms the regularity of the curvature invariant for all r.
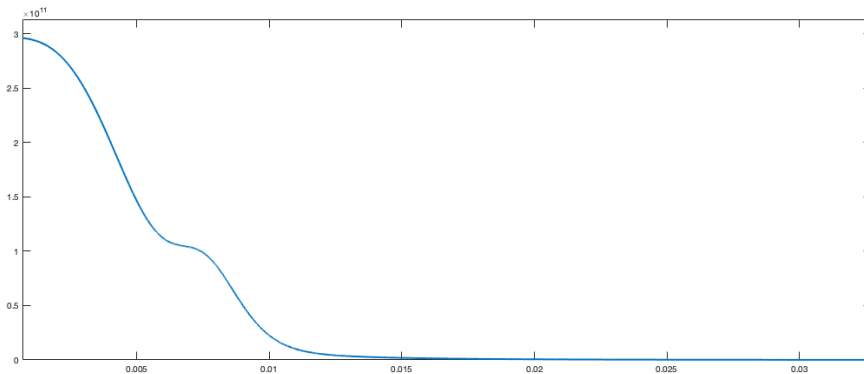

Figure 4.2: $R^{\alpha\beta\gamma\delta}R_{\alpha\beta\gamma\delta}$ plot in Schwarzschild $r - coordinate$

4.4 Avoiding The Singularity

4.4.1 Null Geodesics

As mentioned previously in Chapter 2, the Lagrangian in Eq.(2.17) must be equated to zero for the null geodesics. This equation becomes

$$\frac{E^2}{g(r)} - \frac{\dot{r}^2}{g(r)} - \frac{L^2}{r^2} = 0 \tag{4.4}$$

or alternatively for null radial geodesics,

$$\left(\frac{dr}{d\tau}\right)^2 = E^2 \quad or \quad \frac{dr}{d\tau} = \pm E \tag{4.5}$$

Together with

$$g(r)\frac{dt}{d\tau} = E \tag{4.6}$$

we get

$$\frac{dr}{dt} = \pm g(r) \tag{4.7}$$

Near the singularity region

To illustrate the in-going and outgoing radial null geodesic near the singularity region and near the inner horizon at r_-, we integrate Eq.(4.7), with $g(r)$ given by the expansion in Eq.(3.55), we obtain the illustration in Fig 4.3, indicating the null cones as well.

We notice that near $r = 0$, the geometry is almost Minkowskian, just like the metric expansion in Eq.(3.55) (quoted below) suggests, if we take the $lim\ r \to 0$

$$1 - a^2 = 1 - (\zeta r)^2 \left[1 - \frac{4}{5}\left(\frac{r}{r_*}\right)^3 + \mathcal{O}\left(\left(\frac{r}{r_*}\right)^6\right)\right]$$

What is notable in this result is the *non-inevitability* of the the $r = 0$ point, or what was the 'singularity' in the Schwarzschild metric. As will become apparent in the following section, this 'singularity' will be possibly, but *not necessarily* reached for a given initial energy.
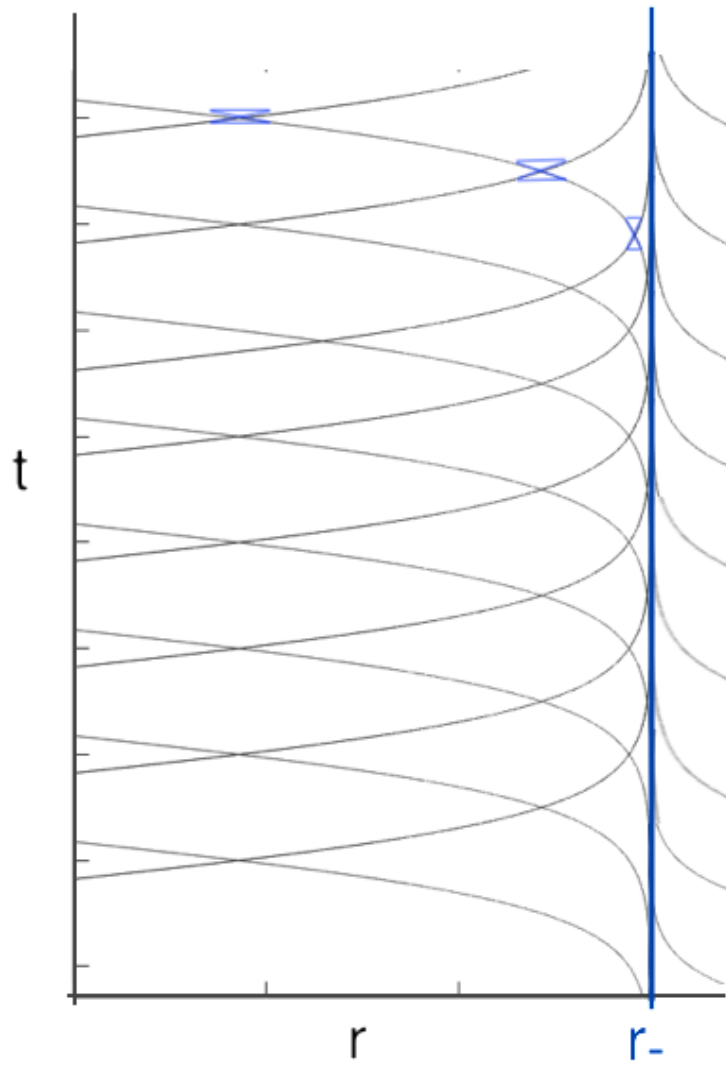
Figure 4.3: Causal Structure of the near singularity region $(0 < r < r_-)$

4.4.2 Time-like Geodesics

From the spatially flat metric given by Eq.(3.52), we set $g(r) = 1 - a^2(r)$, where a is given in Eq.(3.49) in its implicit form. Inserting $g(r)$ and isolating the constants to the RHS to redefine the effective total energy, $\tilde{E}$, Eq.(2.19) becomes

$$\left(\frac{dr}{d\tau}\right)^2 - a^2(r) = \tilde{E}^2 \tag{4.8}$$

Identifying $-a^2(r)$ as an effective potential (V) in the energy expression above, the radial motion is further studied with the plots of $V(r)$ and the resulting phase portrait shown below.
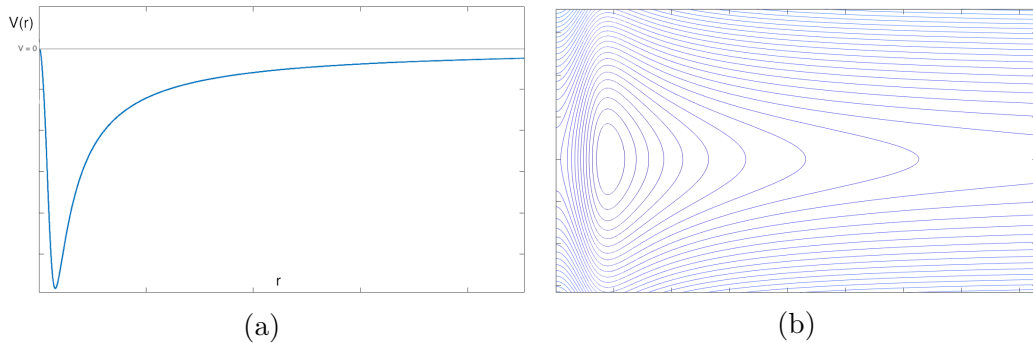

(a)   (b)

Figure 4.4: (a) Effective potential V(r). (b) Phase Portrait for $\tilde{E}^2$ Equation(4.8)

The plots are again obtained by first numerically re-parametrizing $a(\kappa)$ in r-coordinate, aka plotting it vs $b(\kappa)$ given in Eq.(3.50), which is identified as the radial component in Schwarzschild coordinates[reference section], then $a(r)$ is conveniently used in further analysis.

Fixed point at κ_*

As shown before in Eq.(3.51), $a(\kappa)$ admits an extremum at κ_*, or r_* in Schwarzschild coordinates, which is also an extremum for $V(r)$. We can further say that $V(r)$ admits a fixed point at r_*. Using the expansion around r_* provided by the authors in Eq.(3.57), we get that $V'' > 0$ in the region between horizons, implying we can have stable oscillatory motion around r_*.

We get that for different starting energies $\tilde{E}^2$ we observe different types of motion that do not necessarily lead towards the singularity.

For $\tilde{E}^2 = 0$

With foresight, from the phase portrait of Fig 4.4b, we expect the integrated trajectory of this energy to be nothing else but the separatrix. But integrating anyway Eq.(4.8), for $\tilde{E}^2 = 0$, and in the vicinity of $r = 0$ with metric expansion provided by Eq.(3.55), we obtain

$$\tau = \mp \frac{2}{3c} \tanh^{-1} \left[\sqrt{1 - \frac{4}{5}(r/r_*)^3} \right] \tag{4.9}$$

indicating that it will take the particle infinite proper time to reach the center of the NSBH at $r = 0$, if we take the negative sign in the solution indicating in-falling motion. This case doesnt demonstrate, yet, how a particle escapes the 'singularity'(or where it originally was present) at $r = 0$, but it will become apparent in the cases below.

For $\tilde{E}^2 < 0$

We get a trajectory that starts from some starting point r_0 and always meets two turning points, $r_0 := r_{out}$ and r_{in}, say, where $\dot{r}$ vanishes identically. Again, integrating anyway Eq.(4.8), for $\tilde{E}^2 < 0$, and in the vicinity of $r = 0$ with metric expansion in Eq.(3.55), we obtain

$$\tau = \mp \frac{1}{c} \ln \left(c \cdot r + \sqrt{(c \cdot r)^2 - |\tilde{E}^2|} \right) \tag{4.10}$$

From this expression, we see that the particle reaches its turning point in finite time with τ given by solution with a negative sign, and reflects back with its motion described with the same expression above now with a positive sign indicating 'outward' motion, away from the center of the NSBH, thus avoiding the singularity!

For $\tilde{E}^2 > 0$

We get unbound orbits reaching $r = 0$. The particle will simply get reflected off the $r = 0$ point with a switch in velocity sign indicating change of direction. The radial geodesic for $\tilde{E}^2 > 0$ near the 'singularity' is obtained like in the previous case, given by

$$\tau = \mp \frac{1}{c} \ln \left(c \cdot r + \sqrt{(c \cdot r)^2 + \tilde{E}^2} \right) \tag{4.11}$$

So, the particle that arrives from infinity will be 'reflected' near the center of the NSBH,in finite time, and shot out into $r \to \infty$, thus avoiding the singularity, again!

39

4.5 Motion Near the Horizon

From the fixed point obtained at r_*, we concluded that an oscillatory motion *in r direction* is possible, without giving it further regard. Physically, it sounds pretty odd to obtain such a result in which a particle can cross the horizon back from where it entered the first time, and it doesn't seem immediately believable to see such an astronomical structure with particles coming in and out as seen by an observer near the horizon, or worse, particle being shot energetically out of blackholes . Indeed, such a picture of motion near the horizon is incomplete, and is only resolved when we consider the Confromal Diagram specific to our problem.

Extended Conformal diagram of a massive black hole

From [2], the conformal diagram of the family of solutions found in the previous chapter was be obtained by standard methods by gluing the diagrams of the individual regions separated by horizons [17], and is shown below in Fig.(4.5). A detailed form of the extended diagram is given in Fig.(4.6), and will be used for our analysis.
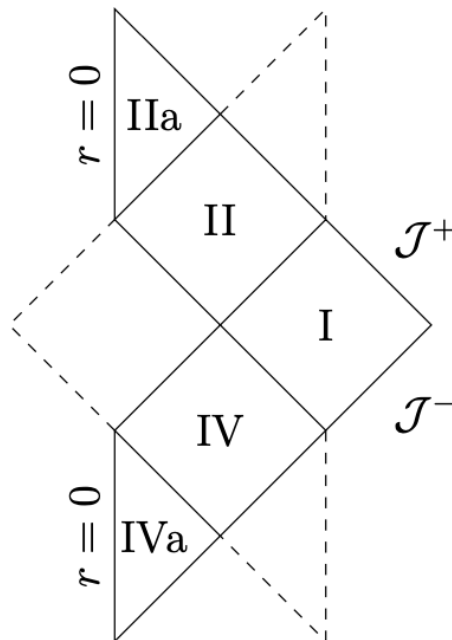

Figure 4.5: Extended Black Hole Conformal Diagram [2]

Description of motion near the horizon

For $\tilde{E}^2 < 0$

In a manifold with horizons, a particle moving between two turning points along its radial time-like geodesic, is in fact moving towards future regions in the Conformal Diagram, as illustrated by the trajectory in **red**. A particle falling from $r_{out} \in region$ I, will arrive to $r_{in} \in region$ IIa in finite time, therefore passing through the Black-Hole. Now, at the next turning point r_{in},the particle will move 'back' and towards increasing r, but 'forward' in the increasing time direction, now passing the White-Hole region IV'. Again, as the particle moves, it reaches the turning point r_{out} in region I, and then starts falling towards decreasing r, to get into the next Black-hole II', continuing this motion ad infinitum. Formally, this motion upward in the Conformal diagram is nothing but the oscillation of the particle between r_{out} and r_{in} in its bound orbit. And every time the particle crosses the outer Horizon r_+ to meet its turning point r_{out}, it is reaching a region of asymptotically flat space, identical to region I, but with its own future infinity, and causally disconnected from previous regions I, therefore as if it had crossed into a 'new Universe'!

For $\tilde{E}^2 > 0$

Similarly, a particle which starts at $r = \infty$ ($\mathcal{J}^-$), crosses the outer and inner horizons, reaches $r = 0$ in finite time, and crosses the inner and outer horizon again, now present in the future time direction on the conformal diagram, and travels along its trajectory shown in **blue** in Fig.4.5, to $r = \infty$ laying in its future ($\mathcal{J}^+$) in the asymptotically flat universe I'.

In the two previous cases, this information of crossing particles lies in the absolute future of external observers and remains forever inaccessible for them. Hence, their degeneracy should not lead to any paradoxes in calculating physical processes observed by external observers.

For $\tilde{E}^2 = 0$

Even though we don't encounter any contradictions while looking at the physical scenario for a particle with $\tilde{E}^2 = 0$, we can still relate it's motion to the conformal diagram, for a complete picture of all our possible scenarios. A particle that starts at i^-, will pass outer and inner horizon and after **infinite** proper time it will reach $\widetilde{i^+}$ ($T = \infty, r = 0$).

Figure 4.6: Extended Black Hole Conformal Diagram

4.6 Non-Radial Motion

To give a complete picture of particle motion (both massive and mass-less) in the field of our non-singular black hole, in contrast to the classical picture in a Schwarzschild scenario, a semi-quantitative analysis of non-radial geodesics will be provided below-which is again, due to the absence of an analytic expression for the metric function.

4.6.1 Time-like Geodesics

Time-like geodesics can be analyzed by considering $\dot{r}^2$ in Eq.(2.17) as the kinetic-energy term, and consequently, we got the energy expression given by Eq.(2.18)

$$\left(\frac{dr}{d\tau}\right)^2 + g(r)\left(1 + \frac{L^2}{r^2}\right) = E^2$$

where the potential $V(r)$ is given by

$$g(r)\left(1 + \frac{L^2}{r^2}\right) \tag{4.12}$$

and the condition for allowed motion is specified by $E^2 \geq V(r)$.

Extrema of the potential where $V'(r) = 0$ determine the circular orbits, and satisfy

$$g'(r)\left(1 + \frac{L^2}{r^2}\right) + g(r)\left(-2\frac{L^2}{r^3}\right) = 0$$

or

$$g'(r)\left(r^3 + r \cdot L^2\right) - 2g(r) \cdot L^2 = 0 \tag{4.13}$$

The plot for the general shape of such a potential is given in Fig.(4.7), it is plotted for a $M > M_{min}$ and $L > \sqrt{12}M$. The plot is out of scale to be able to show its features which can't be captured at the same scale, and instead are shown in separate figures scaled appropriately in Fig.(4.8), taking different L/M values.

Potential Characteristics

The first thing we notice is the positive asymptote as $r \to 0$ which creates an extra well in the potential.

For this massive black hole case ($M > M_{min}$), the potential curve $V(r)$ has two extrema for $r > r_+$ and are very similar to those in the regular Schwarzschild geometry where the shape of the potential does not depend on the black hole mass [7].
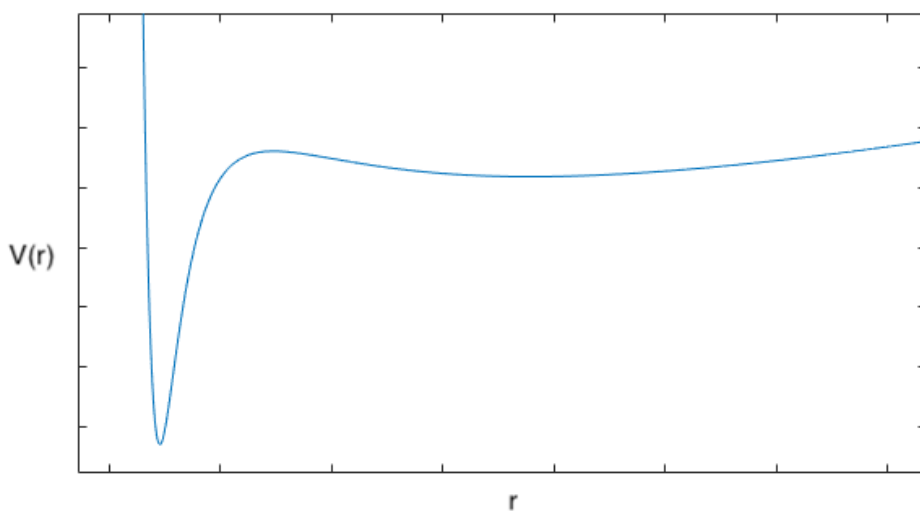

Figure 4.7: General Metric Form for effective potential $V(r)$ for $M > M_{min}$

The fixed points and orbits obtained in Schwarzschild-de Sitter geometry will be discussed below.

Effective Potential Regions in Fig.4.9 and Fig.4.8

As mentioned earlier, given the different scales on which certain potential characteristics appear in the numerical plot where the exact metric function is used, the potential was appropriately split into 3-regions which capture the essential features.
Region $r > r_+$ showing a stable point — shown in marked region in Fig.4.8c, and the exact numerical plots for that region are shown in Fig.4.9c.
Region $r > r_+$ showing unstable point — shown in marked region in Fig.4.8b, and the exact numerical plots for that region are shown in Fig.4.9b.
Region $r_- < r < r_+$ showing a stable point — shown in marked region in Fig.4.8a, and the exact numerical plots for that region are shown in Fig.4.9a.

Classical Schwarzschild Orbits

We obtain the same set of solutions in the Schwarzschild region of our solution ($r > r_+$), namely two fixed points (a stable and an undstable one), for which we obtain the usual stable orbits for $L > \sqrt{12}M$ around the stable fixed point given by $V'(r) = 0, V''(r) > 0$, as shown in Figs. 4.8c and 4.9c, for an appropriate energy condition. These fixed points similarly merge for $L = \sqrt{12}M$ as can be seen in Fig.4.9b and beyond which any incoming particle is necessarily pulled into $r = r_+$ and undergoes a similar motion to that described in Sec.4.4.2.

New Class of Bound Orbits

We can immediately see from Eq.(4.13) that in the de Sitter region, for $r < r_-$, $g'(r) < 0$ and $g(r) > 0$, and therefore bound orbits cannot exist in this region of space-time beyond the internal horizon (IIa). However, we do obtain a stable point in the region $r_- < r < r_+$, which exists for all L, as shown in 4.9a, implying a new class of bound orbits obtained in our peculiar non-singular metric.

The new-type geodesic oscillates between some point, say, r_1 in region IIa where $0 < r_1 < r_-$, and r_2 in region I ($r_2 > r_+$). We classify this geodesic as a bound orbit of the type that climbs the coformal diagram space-time ladder as do bound radial trajectories discussed earlier. A particle starting from the point $r = r_2 \in$ I crosses the NSBH event horizon r_+, the horizon r_- and meets a turning point $r_1 \in$ IIa. Then the particle moves through the white hole region IV' to the next region I'. Formally, this is a bound orbit, $r_1 \leq r \leq r_2$, but in fact, the particle travels upwards the conformal diagram, towards future asymptotically flat regions.

A general consequence of regularity of the center of our Non-Singular BH solution is the existence of innermost stable orbits for particles, and not only for massive particles, as we will show in the next Section.
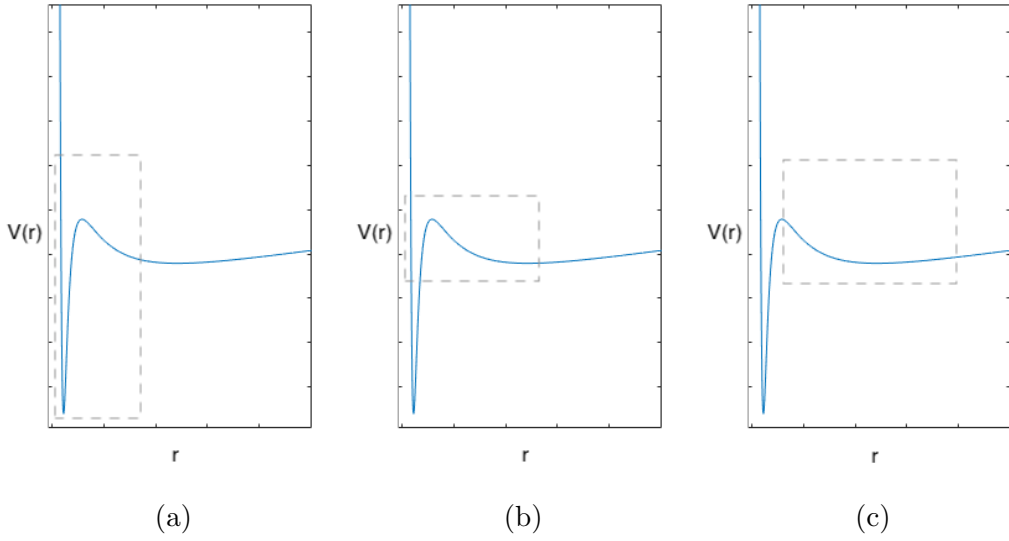
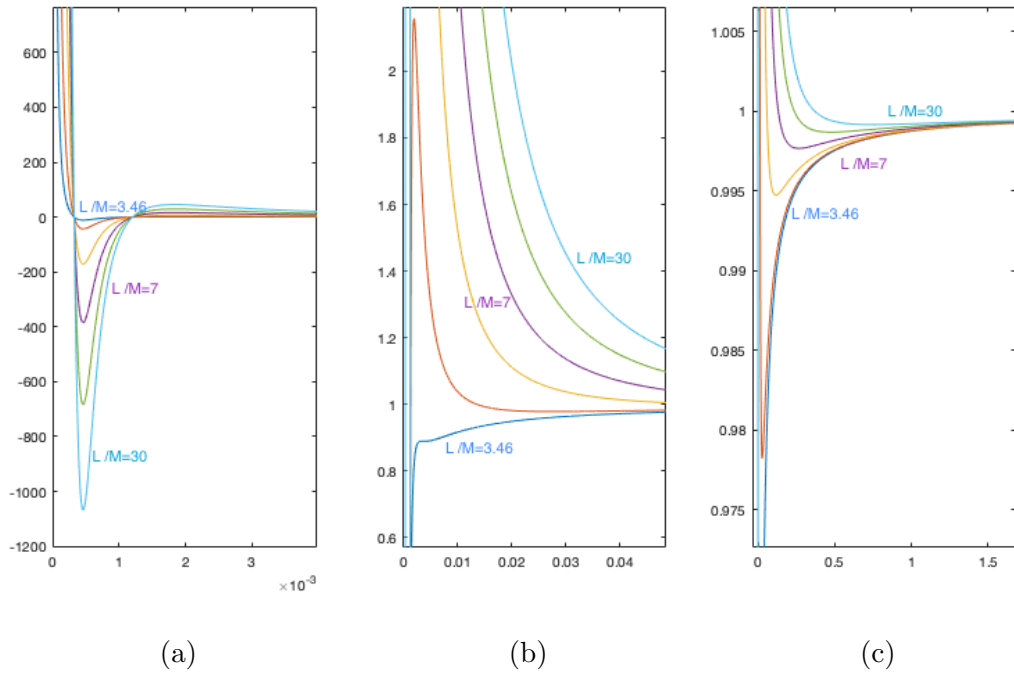Figure 4.8: Plots specifying focus regions expanded for $V(r)$ in Fig.4.9

Figure 4.9: (a) 'Pit in the potential' for $r_- < r < r_+$. (b) Last stable orbit for $r > r+$ occurring right before $L = \sqrt{12}M$. (c) Schwarzschild-like 'potential well' for $r > r_+$.

46

4.6.2 Photon Orbits

Recall that the Energy expression for a photon is given by Eq.(2.33)

$$\left(\frac{dr}{d\lambda}\right)^2 + B^{-2}(r) = b^{-2} \tag{4.14}$$

where the effective potential for photons is

$$B^{-2}(r) = g(r) \cdot r^{-2} \tag{4.15}$$

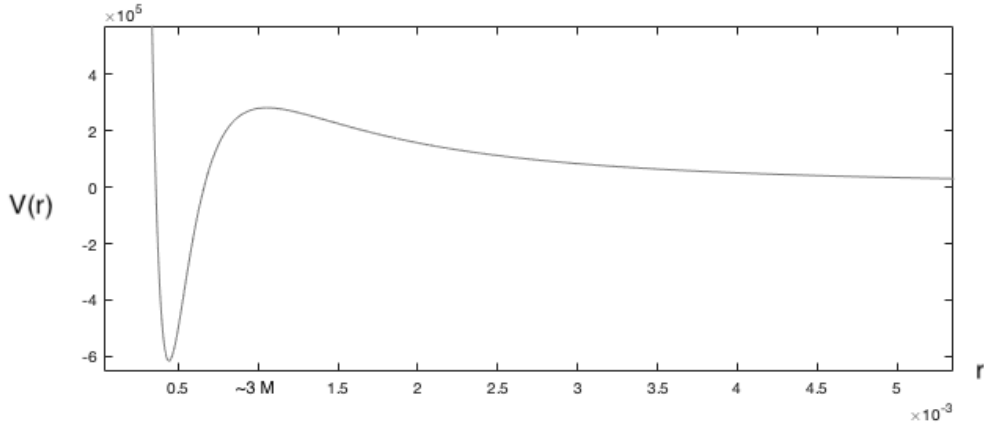The diagram for $B^{-2}(r)$, obtained numerically, is shown in Fig.4.10

Figure 4.10: Effective Potential Diagram for a Photon

According to Eq.(4.15), the typical behavior of the potential $V(r) := B^{-2}(r)$ is determined by the generic behavior of the metric function $g(r)$. The potential $V(r) \to \infty$ as $r \to 0$ where $g(r) \to 1$. It is evident that the generic behavior of the potential at $r \to 0$ leads to that its first extremum is the minimum.

Just like in the effective potentials studied earlier, beyond the outer horizon at $= r_+$, where the solution is asymptotically Schwarzschild, we expect to see an overlap in the description of motion in its effective potential. And in this as well, the photon effective potential matches the description of that in the Schwarzschild case, where we have an unstable maximum in the potential occurring where $b^{-2} = B^{-2}(r_{unstable\ extremum}) := B^{-2}_{crit}$ at $r := r_{crit} \approx 3M$ [1]; this etxremum occurs in region I.

For $b^{-2} < B_{crit}^{-2}$ in Region I

The type of motion for a photon with $b^{-2} < B_{crit}^{-2}$, or $b > 3\sqrt{3}M$, was discussed in Sec.2.2.2.

For $b^{-2} > B_{crit}^{-2}$

For $b^{-2} > B_{crit}^{-2}$, there's an unbound orbit with a turning point $r \in region$ IIa. An orbit starting at infinity crosses both horizons, then the photon 'reflects of the potential barrier' in IIa and travels further up in the conformal diagram to the asymptotically flat region I.

For $b^{-2} < B_{crit}^{-2}$ in Regions $I \cup II \cup IIa$

For and an orbit at which the null geodesic oscillates between its turning points $r_{(\gamma)1}$ and $r_{(\gamma)2}$, the photons travels upward the conformal diagram.

Once again, the de Sitter-Schwarzschild solution admits interesting extra features, and in this case *stable photon orbits*!

4.7 Blackhole Remnants

We know from Sec.(3.4.3) that for $M = M_{min}$, the metric shown in Fig.4.1 transforms further, where the outer horizon r_+ and inner horizon r_- merge at $r_* = r_- = r_+$. This minimal blackhole mass was shown in [18] to be the final product of black hole evaporation, and is a stable minimal remnant with $M = M_{min}$ and vanishing Hawking temperature.

Prelude on Black Hole Thermodynamics

The Hawking temperature T_H is determined by the surface gravity at the exterior horizon x_+. It was found that [18]

$$T_H = \frac{g_s}{2\pi} = \frac{\kappa_0}{6\pi} \, |\tilde{\kappa}_+| \, \frac{1 - 5\tilde{\kappa}_+^2}{1 + 3\tilde{\kappa}_+^2}, \tag{4.16}$$

where $\tilde{\kappa}_+ = \tilde{\kappa}(x_+) \in (-1/\sqrt{5}, 0)$. Since $a(\tilde{\kappa}_+) = 1$, and M can be expressed also through $\tilde{\kappa}_+$ as

$$M = \frac{3}{4\kappa_0 |\tilde{\kappa}_+| (1 - \tilde{\kappa}_+^4)} \left(\frac{1 + 3\tilde{\kappa}_+^2}{1 + \tilde{\kappa}_+^2} \right)^2. \tag{4.17}$$

The formulae (4.16) and (4.17) implicitly define the relation $T_H(M)$. In particular, at large mass we reproduce in leading order the familiar Hawking formula

$$T_H = \frac{1}{8\pi M} \left[1 + \mathcal{O}\left(\left(\frac{M_{min}}{M} \right)^2 \right) \right]. \tag{4.18}$$

Instead of diverging as $M \to 0$, the temperature reaches its maximum value $T_{max} \sim 10^{-2}\kappa_0$ at $|\tilde{\kappa}_+| \approx 0.23$ which corresponds to $M = M_c \approx 1.32 M_{min}$. At this point the negative heat capacity diverges and becomes positive for $M < M_c$. Close to the minimal mass the temperature decreases as

$$T_H \propto \sqrt{M - M_{min}}. \tag{4.19}$$

According to the Stefan-Boltzmann law, the rate of energy loss of a radiating body is determined by $\frac{dM}{dt} \propto -T_H^4 A$ where $A = 4\pi r_+^2$ is the horizon area. For an evaporating black hole close to minimal mass $A \sim M_{min}^2$, and hence it will eventually approach M_{min} according to $M(t) - M_{min} \propto t^{-1}$. That is, the final product of black hole evaporation is a stable minimal remnant with $M = M_{min}$ and vanishing Hawking temperature.

Conformal Diagram

The conformal diagram for the remnant with $M = M_{\min}$ given in [2], is shown below. The space-time structure is now composed of an asymptotically flat region I and a de Sitter core IIa only. A black hole-like region II and a white hole-like region are completely absent in this space-time.
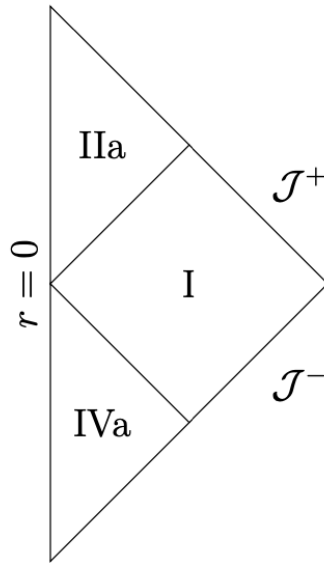

Figure 4.11: Minimal Black Hole Conformal Diagram [2]

EXtended CD for a minimal NSBH

However, we shall deduce the structure of the *extended* conformal diagram of a NSBH remnant by taking the limit $r_- = r_+$ in the extended diagram provided in Fig.(4.6). The resultant diagram is shown in Fig.(4.12). We obtain an extended structure to match the bound motion in r which will be obtained analogously to the results in Sec.(4.4.2).
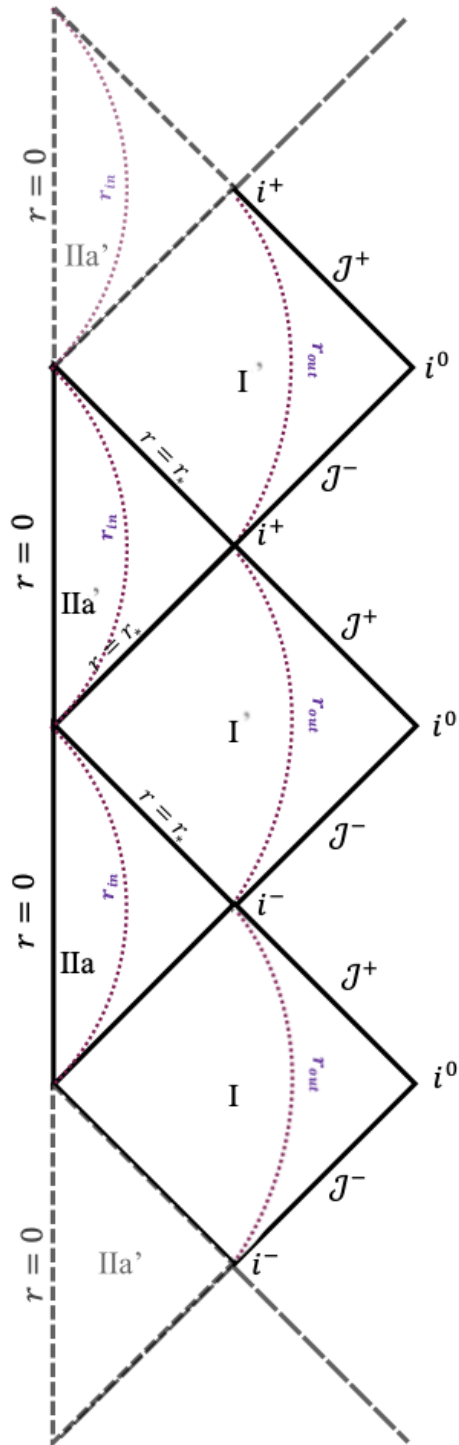
Figure 4.12: Minimal Black Hole Extended Conformal Diagram

51

Radial Motion

The radial time-like geodesics can be thus obtained from Eq.(4.8), quoted below

$$\left(\frac{dr}{d\tau}\right)^2 - a^2(r) = \tilde{E}^2$$

The shape of the effective potential is just like the one shown in Fig.(4.4a), because as the equation above suggests, the effective potential $V(r)$ in the problem has the shape of the metric function $(a^2(r))$. The only difference in the radially in-falling motion in the field of this minimal NSBH case than that of a massive NSBH discussed earlier in Sec.(4.5), is that the fixed point coincides with the horizon at $r = r_*$. The radial oscillation is thus limited to the only two regions now present in the causal diagram of the BH remnant (regions I and IIa).

Just like before, a particle with $\tilde{E}^2 < 0$ starts its motion from an $r = r_{out}$ in region I of its space-time (Fig.(4.12)), crosses the horizon at $r = r_*$ and reaches its turning point $r = r_{in}$ in region IIa, and moves further up the conformal diagram, crossing the horizon again, now present in the future direction, and reaches its turning point r_{out} in the asymptotically flat region I, and continues this bound motion, climbing further up on the diagram.

(a)   (b)   (c)
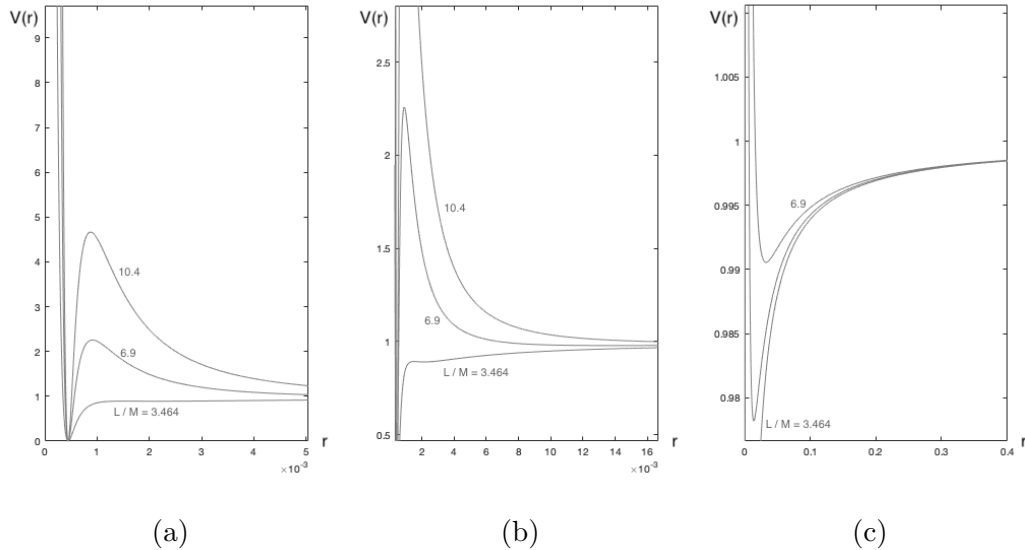
Figure 4.13: (a) Additional 'Pit in the potential' with a minimum at r_*. (b) Last stable orbit vanishing for $L = \sqrt{12}M$. (c) Schwarzschild-like potential well for $r > r_+$.

Non-Radial Motion

For completeness, the different characteristic regions of the effective potential V(r) for non radial motion, discussed in Sec.(4.6) given by Eq.(4.12) quoted below, are shown in Fig.(4.13).

$$V(r) = g(r)\left(1 + \frac{L^2}{r^2}\right)$$

Here, the new fixed point is at $r = r_*$, which means any *new* bound orbits obtained will be of the bound type oscillating between different space time regions, and again in this case these are regions I and IIa.

Similarly to the non-radial time-like motion discussed in Sec.4.6, the last stable orbit orbit in the region $r > r_+$ vanishes at $L = \sqrt{12}M$, just like in the classical Schwarzschild problem, as shown in Fig.4.13b.

Photon Orbits

Following the same analysis done in Sec.4.6.2, and looking at the effective potential for the BH remnant with $M = M_{min}$ presented in Fig.4.14, the general characteristics of the photon orbits will be the same as for the massive NSBH, with one difference which is that the stable extremum in the potential occurs exactly at the horizon (r_*) of this minimal mass NSBH.
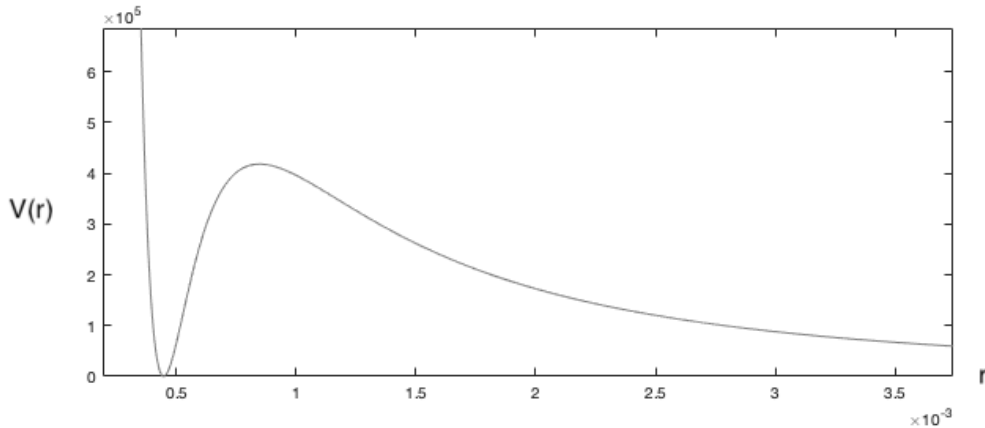

Figure 4.14: Effective Potential for a Photon in the field of a BH Remnant

4.8 Gravitating Solitons

The case with $M < M_{min}$ presents especially interesting results, even though there is no realized mechanism in which this mass limit can be attained, since as discussed in the previous section, the black hole evaporation yielded a remnant with minimal mass M_{min} which is stable, but in fact the theory does not prohibits the existence of lower mass limits $M < M_{min}$. Regardless, we will study interesting properties of this solution in the same formalism in which other mass limits were studied in previous Sections.

Confromal Diagram

The major difference between the conformal diagram [2] for the $M < M_{min}$ mass limit is that it does not admit any horizon and the causal structure is just like Minkowski spacetime. Close to $r = 0$ the solution approaches a static de Sitter metric replacing the singularity.. The immediate result is that any non-typical motion occurring in the field of this gravitating mass will be possibly observable. The conformal diagram is shown in Fig.4.15.

Radial Motion

In contrast to the previously discussed radial time-like motion in NSBHs in Sec.4.5 and Sec.4.7, the radially bound motion around the fixed point r_*, and any other motion, is fully contained in region I which is fully accessible to external observers.
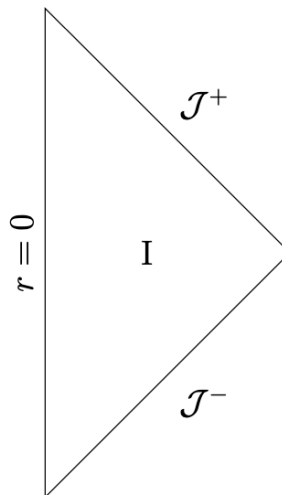

Figure 4.15: Minimal Black Hole Conformal Diagram [2]

Non-Radial Moion

There are two mass limits featuring different behavior in their full potentials within $M < M_{min}$ limit itself. We turn to the effective potential as given by Eq.(4.12), shown in Fig.4.16, but now for different mass limits, while keeping L fixed at a value $L > \sqrt{12}M$ in order to study the additional bound orbits obtain in earlier sections, while keeping the regular ones obtained in a classical Schwarzschild effedctive-potential present.

We see that for a mass $M < M_{crit} < M_{min}$, the 'additional' pit in the potential vanishes, but for a range of masses $M_{crit} < M < M_{min}$, it is still present, indicating that the new class of bound stable orbits obtained idenitically in NSBHs with $M \geq M_{min}$ is present in this gravitating low-mass structure, and is in pronciple observable!

To identify M_{crit}, we can in principle look at the plots of the position of r_*, r_+, and r_-, where r_+ and r_- don't hold any real meaning in this scenario without horizons, but they will serve as the critical parameter which defines M_{crit}. The figure showing r_*, r_+, and r_- plotted against M/M_{min} is shown in Fig.4.16c. We notice that as M/M_{min} decreases, r_+ and r_- become closer and eventually converge at one point, and then diverge as $M \to 0$. The point at which r_+ and r_- converge defines a critical mass M_{crit} beyond which no additional stable orbits are present. For $M < M_{crit}$, the potential admits only one stable fixed point shown in Fig.4.16b, where the unstable point that is similar to the one in a Schwarzschild potential vanishes too. This pit in the potential doesn't vanish for any L, and in fact, as $L \to 0$, the effective potential takes the shape of that of a radially in-falling point and formally has the form of the metric function g(r) shown in Fig.4.1.

Photon Orbits

As we have already established, the low-mass gravitating structure has a critical mass limit which is also apparent in the signature of the 'effective potential of photons'. As can be seen in Fig.4.16d, there is a pit in the potential, similar to ones obtained for $M \geq M_{min}$ limits, for $M_{crit} < M < M_{min}$. Beyond that, for $M < M_{crit}$, this pit in the potential vanishes, and with it the extremum which is reminiscent from the Schwarzschild case.

This is a notable feature which is obtained in this gravitating sturcture without horizons: the existence of stable bound photon orbits in the space-time region accessible for external observers!
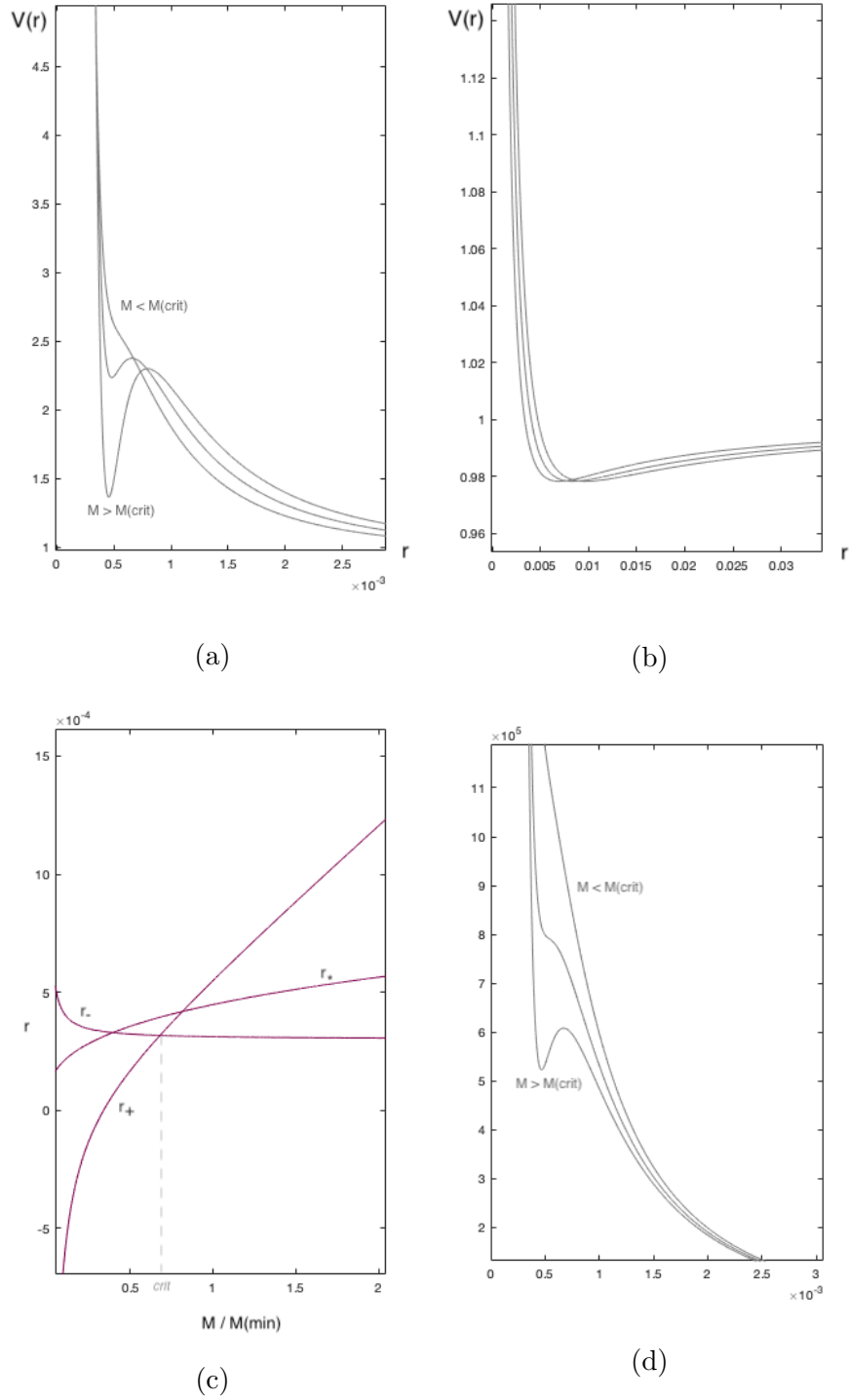
Figure 4.16: (a)Mass-dependent potential for the Gravitating Soliton. (b) Potential for $M < M_{crit}$. (c) Plot of positions of r_*, r_+, and r_- varying with M/M_{min}. (d) Effective Potential for photons for different low-mass limits.

Chapter 5

Conclusion and Future Work

The introduction of the mimetic field ϕ by the authors in [2] allowed them to find a remarkably simple high-curvature modification of GR, where a scale dependence of gravitational and cosmological constant was implemented covariantly. $\Box\phi$ turned out to be a unique measure of curvature on which the gravitational constant can depend such that the resulting modified Einstein equation is still second order in time. In application to non-rotating black holes, a particularly interesting solution was obtained, which preserves the Schwarzschild limit outside the event horizon, but replaces the singularity with a regular de Sitter core.

This modification allowed us to study the whole spectrum of possible dynamics for massive and massless particles alike, and we obtained rather curious additional fearures in these dynamics. For start, we analyzed the motion of radially in-falling particles, and showed how these particles arrive near the center of the NSBH in finite time (Sec.4.4.2), where the space-time was shown to be asymptotically Minkowskian towards $r = 0$ (Sec.4.4.1), and then were 'reflected' towards upper regions in the conformal diagram (Sec.4.5) , lying outside the causal reach of external observers. For the NSBH with $M \geq M_{min}$. We found interesting behavior for massive particles near the event horizon (Sec.4.5), which was the result of the 'pit in the potential', where particles oscillate in and out of the horizon, but the oscillation is occurring forward in time on the conformal diagram, and hence is out of the reach of an external observer. We also found bound orbits for such particles with non zero angular momentum (Sec.4.6), that exhibit the same type of oscillation near the horizon, but move up the conformal diagram thus avoiding any physical contradictions. A particularly interesting result obtained was stable photon orbits in the inner region of the space-time metric (Sec.4.6.2).

Even though it was found that this modification of GR generically leads to a lower bound on the black hole mass [18], where minimal black holes have vanishing Hawking temperature and the final product of black hole evaporation is hence a stable remnant of minimal mass, this work studied possible dynamics in the limit $M < M_{min}$ (Sec.4.8). This mass limit is not prohibited in the theory, regardless of the fact that the mechanism which leads to a low-mass Gravitating structure is not understood yet. The prominent feature of such a gravitating structure was its space-time with no horizons. This means that the additional features which the metric exhibits on different potentials studied, yielding new dynamics, are potentially observed. The most remarkable result is the presence of stable photon orbits.

A Run Down in History

The idea of resolving the singularity of a black hole through replacing it by a de Sitter core dates back to mid-60s, when Sakharov first suggested that the equation of state at extremely high densities can become $p = -\epsilon$ [19]. Around a year later, Gliner suggested that the final state of a gravitational collapse can be described by a vacuum stress energy tensor which he identified as $T_{\mu\nu} = \Lambda g_{\mu\nu}$ [20]. Later Zel'dovich understood that de Sitter geometry, hence the cosmological constant is generated by vacuum with energy density $\epsilon \propto \Lambda$ [21]. The picture comes together even more with Markov, suggesting that the scale of replacing a black hole singularity by a de Sitter-like core can be of Planckian scale [22]. One of the immediate applications of this sequence of ideas was in a paper written by Frolov, Markov and Mukhanov (FMM) in 1990, where they constructed the de Sitter-Schwarzschild metric by direct matching of the the outside Schwarzschild solution to the de Sitter solutoin inside through a joint layer, using a thin shell approach [23]. In their paper, FMM used a mass function $m(r)$ in the metric, where it is proportional to m for $r \to \infty$, and for $r \to 0$, $m(r) \sim r^3/2l^2$; later they suggest that this mass function can be equally mimicked by a vanishing gravitational constant. This realization, together with the discussed asymptotically free theory on which this thesis is based on, will be relevant once one last work is mentioned in the historic chain of the problem. In a paper in 1992 [24], Dymnikova used an analytic expression for a density function which returns the mass of the black hole at $r \to \infty$, and the energy density of vacuum at the center of the black hole, and was able to obtain the explicit metric for a non-singular black hole solution which is a smooth transition from de Sitter to Schwarzschild at the appropriate limits, in contrast to the implicit solution obtained in [2].

Projection into Future Work

Since part of the analysis on orbits was done semi-quantitatively due to the limiting fact that the metric provided by [2] is an implicit function in κ, and the discussion was based on numeric plots of needed functions, a more rigorous numeric study is needed to study the orbits obtained and their features. However, there is a similar numeric analysis of orbits done in the work by [25], for a non-singular metric function similar to the one which on this work is built. And while the non-singular solution in [24], as mentioned earlier, was obtained by assuming a certain analytical expression for mass distribution inside a black hole, it would also be interesting to investigate a possibly exact non-implicit solution that can be obtained by assuming a mass distribution for the mimetic dark matter, in Chamseddine and Mukhanov's theory, which is left out as an integration factor in [8], without having to assume anything about the state of matter at high densities [19].

Indeed, if we plot the function of the running Gravitational constant that the authors introduce into their modified Lagrangian (3.4) through its inverse, we can see a good match between that and a theorized mass function for mimetic dark matter, similar to that in [24], given by a general function $M(r) = 1 - e^{-(r/a)^3}$,where a is a constant that fitted appropriately. This plot is shown in Fig.5.1.

While the vanishing mass distribution, or the gravitational constant alike, are not enough to obtain a de Sitter core replacing the singularity-which requires the addition of a cosmological like term like in Eq.(3.4), or by including vacuum density appearing asymptotically in the mass function as in [24], if we want to get a de Sitter core from mimetic dark matter, we need to alter its properties. It is readily seen from [8] that the equation of state of the mimetic dark matter in the theory has $p = 0$, which came as a consequence of isolating the scalar field in the physical metric, so in principle it cannot be simply modified. However, in another work by the authors in 2014 [26], a cosmological constant term was introduced as a Lagrange multiplier constraining a potential depending on ϕ. While such a ϕ-dependent potential turned out to be problematic later on, turning back to this approach is not the simplest, but the least can be thought of as a starting point to thinking about how to obtain a dS-Schw solution purely from mimetic dark matter, without altering properties of the gravitational constant, or matter itself in that respect.
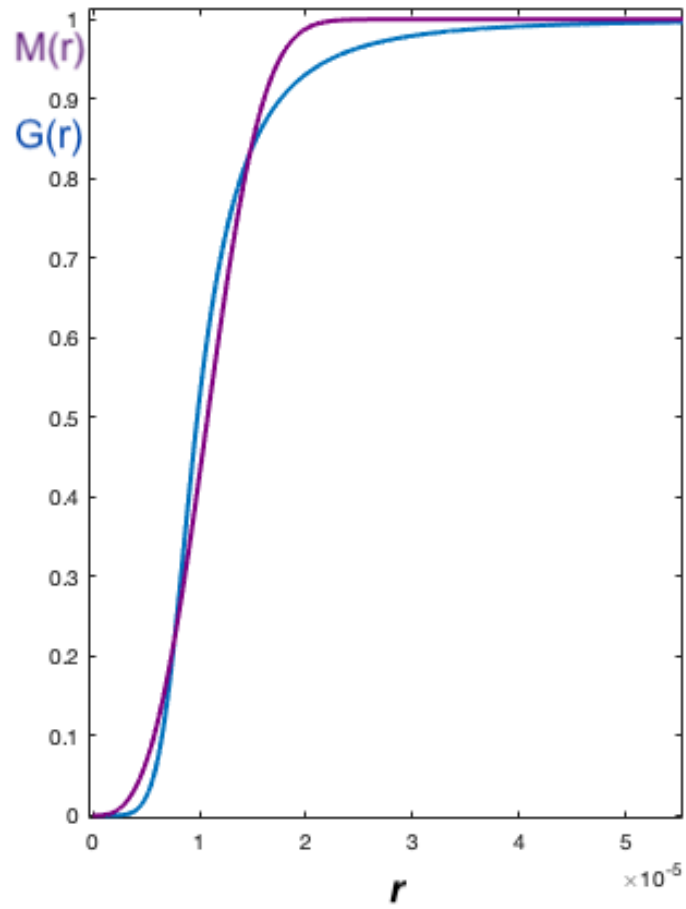
Figure 5.1: A general Mass function $M(r)$ fitted to running Gravitational constant from [2]

Bibliography

[1] K. S. Thorne, C. W. Misner, and J. A. Wheeler, *Gravitation*. Freeman, 2000.

[2] A. H. Chamseddine, V. Mukhanov, and T. B. Russ, "Non-flat universes and black holes in asymptotically free mimetic gravity," *Fortschritte der Physik*, vol. 68, no. 1, p. 1900103, 2020.

[3] J. R. Arenas, "Nobel prize in physics 2020," *MOMENTO*, no. 62, 2021.

[4] S. W. Hawking and R. Penrose, "The singularities of gravitational collapse and cosmology," *Proceedings of the Royal Society of London. A. Mathematical and Physical Sciences*, vol. 314, no. 1519, pp. 529–548, 1970.

[5] M. Markov, "Limiting density of matter as a universal law of nature," *ZhETF Pisma Redaktsiiu*, vol. 36, pp. 214–216, 1982.

[6] M. Markov and V. F. Mukhanov, "De sitter-like initial state of the universe as a result of asymptotical disappearance of gravitational interactions of matter," *Il Nuovo Cimento B (1971-1996)*, vol. 86, no. 1, pp. 97–102, 1985.

[7] S. Chandrasekhar, *The mathematical theory of black holes*, vol. 69. Oxford University Press, 1998.

[8] A. H. Chamseddine and V. Mukhanov, "Mimetic dark matter," *Journal of High Energy Physics*, vol. 2013, no. 11, p. 135, 2013.

[9] A. H. Chamseddine, A. Connes, and V. Mukhanov, "Quanta of geometry: noncommutative aspects," *Physical review letters*, vol. 114, no. 9, p. 091302, 2015.

[10] A. H. Chamseddine, "Quanta of space-time and axiomatization of physics," in *Foundations of Mathematics and Physics One Century After Hilbert*, pp. 211–251, Springer, 2018.

[11] A. Golovnev, "On the recently proposed mimetic dark matter," *Physics letters B*, vol. 728, pp. 39–40, 2014.

[12] A. H. Chamseddine, V. Mukhanov, and T. B. Russ, "Asymptotically free mimetic gravity," *The European Physical Journal C*, vol. 79, no. 7, p. 558, 2019.

[13] V. Mukhanov and R. Brandenberger, "A nonsingular universe," *Physical review letters*, vol. 68, no. 13, p. 1969, 1992.

[14] R. Brandenberger, V. Mukhanov, and A. Sornborger, "Cosmological theory without singularities," *Physical Review D*, vol. 48, no. 4, p. 1629, 1993.

[15] A. G. Lemaître and A. S. Eddington, "The Expanding Universe," *Monthly Notices of the Royal Astronomical Society*, vol. 91, pp. 490–501, 03 1931.

[16] E. Poisson, *A relativist's toolkit: the mathematics of black-hole mechanics.* Cambridge university press, 2004.

[17] V. Mukhanov and S. Winitzki, *Introduction to quantum effects in gravity.* Cambridge University Press, 6 2007.

[18] A. H. Chamseddine, V. Mukhanov, and T. B. Russ, "Black hole remnants," *Journal of High Energy Physics*, vol. 2019, Oct 2019.

[19] A. D. Sakharov, "The initial stage of an expanding universe and the appearance of a nonuniform distribution of matter," *Sov. Phys. JETP*, vol. 22, pp. 241–249, 1966.

[20] E. B. Gliner, "Algebraic properties of the energy-momentum tensor and vacuum-like states o+ matter," *Soviet Journal of Experimental and Theoretical Physics*, vol. 22, p. 378, 1966.

[21] Y. B. Zeldovich *Sov. Phys. Uspekhi*, vol. 95, p. 268, 1968.

[22] M. A. Markov *Sov. Phys. Lett.*, vol. 36, p. 265, 1982.

[23] V. P. Frolov, M. Markov, and V. F. Mukhanov, "Black holes as possible sources of closed and semiclosed worlds," *Physical Review D*, vol. 41, no. 2, p. 383, 1990.

[24] I. Dymnikova, "Vacuum nonsingular black hole," *General relativity and gravitation*, vol. 24, no. 3, pp. 235–242, 1992.

[25] I. Dymnikova, A. Poszwa, and B. Sołtysek, "Geodesic portrait of de sitter-schwarzschild spacetime," *Gravitation and Cosmology*, vol. 14, no. 3, pp. 262–275, 2008.

[26] A. H. Chamseddine, V. Mukhanov, and A. Vikman, "Cosmology with mimetic matter," *Journal of Cosmology and Astroparticle Physics*, vol. 2014, no. 06, p. 017, 2014.